Biogeosciences
Discussions

Assessing the value of BGC Argo profiles versus ocean colour observations for biogeochemical model optimization in the Gulf of Mexico

Bin Wang[1], Katja Fennel[1], Liuqian Yu[1,2], Christopher Gordon[1]

[1]Department of Oceanography, Dalhousie University, Halifax, Nova Scotia, Canada

[2]Department of Mathematics, The Hong Kong University of Science and Technology, Kowloon, Hong Kong

Correspondence to: Bin Wang (Bin.Wang@dal.ca)

Abstract. Biogeochemical ocean models are useful tools subject to uncertainties arising from simplifications, inaccurate parameterization of processes, and poorly known model parameters. Parameter optimization is a standard method for addressing the latter but typically cannot constrain all biogeochemical parameters because of insufficient observations. Here we assess the trade-offs between satellite observations of ocean colour and biogeochemical (BGC) Argo profiles, and the benefits of combining both observation types, for optimizing biogeochemical parameters in a model of the Gulf of Mexico. A suite of optimization experiments is carried out using different combinations of satellite chlorophyll and profile measurements of chlorophyll, phytoplankton biomass, and particulate organic carbon (POC) from autonomous floats. As parameter optimization in 3D models is computationally expensive, we optimize the parameters in a 1D model version, and then perform 3D simulations using these parameters. We show first that the use of parameters optimized in 1D improves the skill of the 3D model. Parameters that are only optimized with respect to surface chlorophyll cannot reproduce subsurface distributions of biological fields. Adding profiles of chlorophyll in the parameter optimization yields significant improvements for surface and subsurface chlorophyll but does not accurately capture subsurface phytoplankton and POC distributions because the parameter for the maximum ratio of chlorophyll to phytoplankton carbon is not well constrained in that case. Using all available observations leads to significant improvements of both observed (chlorophyll, phytoplankton, and POC) and unobserved variables (e.g. primary production). Our results highlight the significant benefits of BGC Argo measurements for biogeochemical parameter optimization and model calibration.

1. Introduction

28   Oceanic primary production forms the basis of the marine food web and fuels the biological pump,

29   which contributes to the sequestration of atmospheric CO_2 in the ocean's interior thus mitigating global

30   warming. An accurate quantification of primary production and biological carbon export is therefore

31   important for our understanding of the marine carbon cycle and for predicting how carbon cycling and

32   marine ecosystems will interact with climate change.

33   Direct observations of primary production and export flux are relatively sparse because of the cost

34   and effort involved in measuring these fluxes. Numerical models can complement sparse observations.

35   Well validated and calibrated models are useful tools for hindcasting and nowcasting past and present

36   biogeochemical fluxes and are the most common tool for projecting future changes.

37   In recent years, many biogeochemical models with different complexities, ranging from three to more

38   than thirty biological state variables, have been developed to study ocean biogeochemical processes.

39   Regardless of their complexities, the performance of these models is highly dependent on the appropriate

40   choice of model parameter values (e.g. maximum growth, grazing and mortality rates), most of which are

41   poorly known. Some parameter choices are informed by laboratory experiments (e.g. light and nutrient

42   dependence of phytoplankton growth), although isolated cultures in the lab may not be representative of

43   the behavior of natural communities. Other parameters cannot be directly determined (e.g. mortality

44   rates). Choosing appropriate parameter values becomes more challenging as model complexity grows

45   because the number of parameters increases exponentially with the number of state variables (Denman,

46   2003).

47   A standard method for addressing the problem of poorly known model parameters is parameter

48   optimization, a process by which the misfit between model results and available observations is

49   minimized by iteratively varying parameters (Matear, 1995; Prunet et al., 1996a, 1996b; Fennel et al.,

50   2001; Friedrichs et al., 2007; Kuhn et al., 2015, 2018). However, even formal optimization typically

51   cannot constrain all biogeochemical parameters (i.e. provide optimal parameter estimates with relatively

52   small uncertainties) because of insufficient information in the available observations (Matear, 1995;

53   Fennel et al., 2001; Ward et al., 2010; Bagniewski et al., 2011). For example, Matear (1995) used a so-

54 called simulated annealing algorithm to optimize three different ecosystem models and found that even

55 for the simplest nutrient-phytoplankton-zooplankton model, not all independent parameters could be

56 constrained well, leaving the others with large uncertainty ranges. A more recent study reported that the

57 lack of zooplankton observations led to poor accuracy of the optimized zooplankton-related parameters

58 when using a suite of Lagrangian-based observations during the North Atlantic spring bloom (Bagniewski

59 et al., 2011). A broader suite of observation types should be favourable to parameter optimization although

60 complications can arise. For example, when optimizing a suite of 1D models for the Mid-Atlantic Bight,

61 the use of satellite POC observations in addition to satellite chlorophyll did not yield further

62 improvements in model-data fit but degraded the representation of chlorophyll (Xiao and Friedrichs,

63 2014a).

64 Typically surface ocean chlorophyll from satellite is the main source of observations for model

65 validation (e.g. Doney et al., 2009; Gomez et al., 2018; Lehmann et al., 2009) and parameter optimization

66 (Prunet et al., 1996a; Xiao and Friedrichs, 2014a, 2014b), supplemented by other observation types as

67 available. However, satellites only see the ocean surface and do not resolve the vertical distribution of

68 chlorophyll. This is especially problematic in oligotrophic regions where the maximum chlorophyll

69 concentration (referred as the deep chlorophyll maximum, DCM) is pronounced near the base of the

70 euphotic zone because of photoacclimation (Cullen, 2015; Fennel and Boss, 2003). In addition, although

71 chlorophyll has long been used as a proxy of phytoplankton biomass and to estimate primary production

72 based on some assumptions (Behrenfeld and Falkowski, 1997), it is not a direct measure of carbon-based

73 phytoplankton biomass. The ratio of chlorophyll-to-phytoplankton carbon varies by at least an order of

74 magnitude due to physiological responses of phytoplankton to their ambient environment (e.g. nutrients,

75 light, and temperature) (Cullen, 2015; Fennel and Boss, 2003; Geider, 1987). Thus, changes in

76 chlorophyll may result from physiologically induced modifications of the chlorophyll-to-phytoplankton

77 ratio rather than actual changes of phytoplankton biomass (Fommervault et al., 2017; Mignot et al., 2014).

78 Satellite surface chlorophyll alone is therefore likely insufficient for model validation and for constraining

79 biogeochemical models via parameter optimization.

80 Recent advances in autonomous platforms and sensors have opened opportunities for simultaneous

81 measurement of several biological and chemical properties throughout the upper ocean with high

82 resolution, over broad spatial scales and for sustained periods (Roemmich et al., 2019). In particular, the

83 biogeochemical (BGC) Argo program (Johnson and Claustre, 2016; Roemmich et al., 2019) will provide

84 temporally evolving 3D information on biogeochemical variability at previously unobserved scales. Here

85 we assess to what degree observations of chlorophyll fluorescence and particle backscatter from Argo

86 profiles improve the prospects of optimizing a biogeochemical model for the Gulf of Mexico.

87   Since the high computational cost and storage demands of 3D models make direct application of

88 most parameter optimization techniques difficult (but see Mattern et al., 2012; Mattern and Edwards,

89 2017; Tjiputra et al., 2007 for exceptions), they are typically applied in computationally efficient 1D

90 models before using the resulting parameters in 3D version (e.g. Hoshiba et al., 2018; Kane et al., 2011;

91 Kuhn and Fennel, 2019; Schartau and Oschlies, 2003). We follow the latter approach here.

92   The main objective of this study is to assess the added value of bio-optical profile information from

93 Argo floats for biogeochemical model optimization in the Gulf of Mexico. We first examine the feasibility

94 of improving the 3D model by applying the optimal parameters from 1D model optimizations. We find

95 that the gains from the 1D optimizations transfer to the 3D version. Then, by using different combinations

96 of satellite and float observations we show that parameters optimized with respect to satellite data cannot

97 reproduce subsurface distributions unless the float observations (i.e. chlorophyll, phytoplankton, and POC)

98 are also used.

99 **2. Study region**

00   The Gulf of Mexico (GOM) is a semi-enclosed marginal sea (Figure 1) which is characterized by

01 eutrophic coastal waters on the northern shelf and an oligotrophic deep ocean. The high productivity in

02 the northern coastal region is fueled by large nutrient and freshwater inputs from the Mississippi and

03 Atchafalaya Rivers. The large nutrient load and strong stratification driven by Mississippi and

04 Atchafalaya River inputs lead to summer hypoxia and ocean acidification in bottom waters on the

05 northern shelf (Laurent et al., 2017; Yu et al., 2015), but nutrient export across the shelf break into the

06 open Gulf is minor (Xue et al., 2013).

Biogeosciences Open Access
Discussions
EGU

07   The deep ocean of the GOM is oligotrophic. Previous satellite-based studies have revealed a clear

08   seasonal cycle in surface chlorophyll with highest concentrations in winter and lowest in summer

09   (Martínez-López and Zavala-Hidalgo, 2009; Muller-Karger et al., 1991, 2015). Thanks to advances in

10   autonomous profiling technology, recent studies based on simultaneous measurements of subsurface

11   chlorophyll and backscatter have demonstrated that the seasonal variability of surface chlorophyll might

12   be a result of the vertical redistribution of subsurface chlorophyll and/or physiological response to solar

13   radiation of phytoplankton (Fommervault et al., 2017; Green et al., 2014).

3. Methods

3.1. Biological observations

16   Satellite-derived chlorophyll from the Ocean-Colour Climate Change Initiative project (OC-CCI,

17   https://www.oceancolour.org) with a spatial resolution of 4 km from 2010 to 2015 is used for model

18   validation and parameter optimization. These data were provided by the European Space Agency (ESA),

19   which produced a set of validated and error-characterised global ocean-color products by merging

20   SeaWiFS (Sea-viewing Wide Field-of-view Sensor), MODIS (Moderate-resolution Imaging

21   Spectroradiometer), and MERIS (medium-spectral resolution imaging spectrometer) products.

22   In addition to the satellite-based measurements, bio-optical measurements from six autonomous

23   profiling floats are used (Figure 1), which were deployed by the Bureau of Ocean Energy Management

24   (BOEM) and operated in the deep GOM from 2011 to 2015. These floats were equipped with a CTD and

25   bio-optical sensors to collect biweekly profiles of temperature, salinity, chlorophyll fluorescence, and

26   backscatter at 700 nm ($bbp700$ (m^{-1})) from the surface to 1000 m depth (see Fommervault et al., 2017

27   and Green et al., 2014 for more details). Chlorophyll was derived from fluorescence based on the sensor

28   manufacturer's calibrations and cross-validated with the satellite estimates of surface chlorophyll. While

29   the surface chlorophyll measurements from the floats and the satellite estimates both show a typical

30   seasonal cycle and are highly correlated (R^2=0.74; see Figures S1 and S2a in the Supplement), the satellite

31   underestimates the float-measured chlorophyll concentrations in winter (Figure S1c). Satellite estimates

32   were therefore corrected following the regression equation shown in Figure S2a (Figure S1c).

33   The backscatter sensor carried by the floats provides the volume scattering function at a centroid

34 angle of 140° and a wave length of 700 nm ($\beta(140^o, 700nm)$ m^{-1} sr^{-1}) (Green et al., 2014). The profiles

35 were filtered following Briggs et al. (2011) to remove spikes. To cross-validate the float-measured $bbp700$

36 with the satellite estimates, the $bbp670$ from OC-CCI was firstly converted to $bbp700$ through a power

37 law (Boss and Haëntjens, 2016):

$$bbp(\lambda1) = \left(\frac{\lambda1}{\lambda2}\right)^{-\gamma} bbp(\lambda2), \tag{1}$$

41 where $\lambda1$ and $\lambda2$ represent the measured wavelength, and γ was estimated as 0.78 based on the global

42 measurements. Compared to surface chlorophyll, surface $bbp700$ has a less distinct seasonal cycle (Figure

43 S3). For example, the coefficient of variation, defined as the ratio between standard deviation and mean

44 to show the extend of variability, is much lower for $bbp700$ (0.09 and 0.07 for floats and satellite,

45 respectively) than for chlorophyll (0.31 and 0.26 for floats and satellite, respectively). The $bbp700$ from

46 the floats is weakly correlated with the satellite estimates (R^2=0.11) and generally lower by a factor of

47 ~0.45 than the satellite estimates (Figure S2b). The bbp700 profiles were therefore multiplied by 2.2

48 before being converted to $bbp470$ following the equ. 1.

49   Profiles of phytoplankton and POC were derived from the validated $bbp470$ profiles based on the

50 following empirical relationships

$$Phy = 30100 \times (bbp470 - 76 \times 10^{-5})\frac{1}{12 \times 6.625}, \tag{2}$$

$$log10(POC) = 1.22 \times log10(bbp470) + 5.15. \tag{3}$$

56 The relationships for phytoplankton (Martinez-Vicente et al., 2013; equ. 2) and POC (Rasse et al., 2017;

57 equ. 3) were obtained from a data set for the Atlantic Ocean that covers a wide range of oceanographic

58 regimes from eutrophic to oligotrophic ecosystems. The scale factors of 12 and 6.625 in equ. 2 represent

59 the molecular weight of carbon and the Redfield ratio to convert phytoplankton concentrations from mg

60 C m^{-3} to mmol N m^{-3}. According to Behrenfeld et al. (2005), the intercept 76×10^{-5} in equ. 2 represents

61 the background backscatter of nonalgal detritus. In this study, both chlorophyll and phytoplankton

62 approach zero when *bbp470* is 76×10^{-5} m^{-1}, implying that the use of equ. 2 is appropriate.

3.2. 3D model description

64 The physical model is configured based on Regional Ocean Modeling System (Haidvogel et al.,

65 2008; ROMS, https://www.myroms.org) for the Gulf of Mexico (Figure 1). The model has a horizontal

66 resolution of 6~7 km and 36 terrain-following sigma layers with refined resolution near the surface and

67 bottom. The model solves for the horizontal and vertical advection of tracers using the Multidimensional

68 positive definitive advection transport algorithm (MPDATA, Smolarkiewicz and Margolin 1998).

69 Horizontal viscosity and diffusivity are parameterized by a Smagorinsky-type formula (Smagorinsky,

70 1963), and vertical turbulent mixing is calculated by the Mellor-Yamada 2.5-level closure scheme (Mellor

71 and Yamada, 1982). Bottom friction is specified by a logarithmic drag formulation with a bottom

72 roughness of 0.02 m. The model is forced by 3-hourly surface heat and freshwater fluxes, 6-hourly air

73 temperature, sea level pressure and relative humidity, and 10-m winds from the European Centre for

74 Medium-Range Weather Forecast ERA-Interim product with a horizontal resolution of 0.125º (ECMWF

75 reanalysis, https://www.ecmwf.int/en/forecasts/datasets/reanalysis-datasets/era-interim). A bulk

76 parameterization is applied to calculate the surface net heat fluxes and wind stress. The model is one-way

77 nested inside the 1/12º data-assimilative global HYCOM/NCODA (https://www.hycom.org). Tidal

78 constitutes are neglected in the model.

79 The biogeochemical model uses a 7-component model (Fennel et al., 2006) to simulate the nitrogen

80 cycle in the water column. The model describes the dynamics of two species of dissolved inorganic

81 nitrogen (nitrate, NO3, and ammonium, NH4), one function of phytoplankton (Phy), chlorophyll (Chl) as

82 a separate state variable which allows photo-acclimation based on the model of (Geider et al., 1997), one

83 function of zooplankton (Zoo), and two pools of detritus (i.e. small suspended detritus, SDeN, and large

84 fast-sinking detritus, LDeN). Water-sediment interactions are simplified by an instantaneous

85 remineralization parameterization, where detritus sinking out of water column immediately results in a

86 corresponding influx of ammonium into the bottom layer. Detailed descriptions of the model equations

87 can be found in Fennel et al. (2006). The biological model parameters are listed in Table 1.

88   The model receives freshwater, nutrients (NO3 and NH4) and organic matter inputs from major rivers

89 along the Gulf coast. Freshwater and nutrients from the Mississippi and Atchafalaya rivers are prescribed

90 based on the daily measurements by the US Geological Survey river gauges. River particulate organic

91 nitrogen (PON) is assigned to the small detritus pool and determined as the difference between total

92 Kjeldahl nitrogen and ammonium (Fennel et al., 2011). Other rivers utilize the climatological estimates

93 of freshwater, nutrients, and PON as in Xue et al. (2013).

94   Initial and open boundary conditions for NO3 are specified by applying an empirical relationship

95 between NO3 and temperature, derived from the World Ocean Atlas (WOA; Figure S4a), that is applied

96 to the temperature fields from HYCOM/NCODA. Analogously, empirical relationships between

97 chlorophyll and density (Figure S4b), phytoplankton and density (Figure S4c), and POC and density

98 (Figure S4d) were obtained from the median profiles of the bio-optical floats and used to derive initial

99 and boundary conditions for these variables. Zooplankton and small detritus were assumed to amount to

00 10% of phytoplankton biomass and the remaining fractions of POC attributed to large detritus.

01   A 6-year (5 January 2010 – 31 December 2015) hindcast was performed that includes the period of

02 operation of the bio-optical floats. The first year is considered model spin-up and the next five years will

03 be discussed.

04 **3.3. 1D model description**

05   As optimizing a 3D biogeochemical model is computationally expensive, it is more practical to

06 perform the optimization using a reduced-order model surrogate. A surrogate can be a coarser resolution

07 model, a simplified model, or a reduced-dimension model. In this study, a 1D model is used to optimize

08 the biological parameters of the 3D model. This approach has been successfully used previously (Hoshiba

09 et al., 2018; Kane et al., 2011; Oschlies and Schartau, 2005).

10   The 1D model, which is similar to that used by Lagman et al. (2014) and Kuhn et al. (2015), covers

11 the upper 200 m of the ocean with a vertical resolution of 5 m and is configured at one location in the

12 central Gulf (see Figure 1). In the vertical direction, the water column is divided into two layers: the

13 turbulent surface layer and a quiescent layer below. A higher diffusion coefficient ($K_{Z1} =$
14 $\max(H_{MLD}^2/400, 10)$) is applied in the turbulent surface layer and a lower diffusion coefficient ($K_{Z2} =$
15 $K_{Z1}/2$) is assigned to the quiescent bottom layer. The interface between these two layers is determined
16 by the mixed layer depth (H_{MLD}), defined as the depth where the temperature is 5°C lower than at the
17 surface, and was obtained from a simulation of the 3D model. The model is integrated in time using the
18 Crank-Nicolson scheme for vertical turbulent mixing and an implicit time-stepping scheme for the
19 biogeochemical tracers, which are treated identically to the 3D model. Some of the biogeochemical
20 parameterizations require input of temperature and solar radiation, which are also taken from the 3D
21 model. As the 1D model does not consider horizontal and vertical advection, NO3 below 100 m is nudged
22 to that from the 3D base simulation with a nudging time scale of 20 days. The model is run for the year
23 2010 repeatedly for three cycles, with the first two are model spin-up and the last annual cycle used to
24 calculate the misfit between model and observations.

25 **3.4. Parameter optimization method**

26   The evolutionary algorithm described by Kuhn et al. (2015, 2018) is used to search for optimal
27 model parameters by minimizing the misfit between model and observations. The misfit is measured by
28 the following cost function:

29

30
$$F(\vec{p}) = \sum_{v=1}^{V} F_v(\vec{p}), \tag{4}$$

31

32
$$F_v(\vec{p}) = \frac{1}{N_v \sigma_v^2} \sum_{i=1}^{N_v} \left(\hat{y}_{i,v} - y_{i,v}(\vec{p}) \right)^2, \tag{5}$$

33

34 where $\vec{p}$ represents the parameters vector, V is the number of different observation types, N_v is the
35 number of observations for each variable, $F_v(\vec{p})$ is the misfit for observation type v measured as the
36 mean-square difference between observations ($\hat{y}$) and corresponding model estimates ($y(\vec{p})$). The cost

Biogeosciences
Discussions

37   function $F_v(\vec{p})$ is normalized by the standard deviation of each variable type (σ_v) in order to remove the

38   effect of different units.

39   The algorithm is inspired by the rules of natural selection. Following Kuhn et al. (2015), an initial

40   parameter population of 30 parameter vectors is randomly generated within a predefined range of

41   parameters (see Table 1). The model is evaluated for each parameter vector and the resulting cost function

42   is calculated. For this initial generation and each of the following generations, the half of the population

43   with the lower misfit survives into the next generation. The other half is regenerated through a

44   recombination of survivors in a process analogous to genetic crossover. In addition, each newly generated

45   population is subject to random mutations by multiplying the parameter values by a random value

46   between 0 and 2. Parameter values exceeding the predefined range are replaced by their corresponding

47   minimum or maximum limits to avoid unrealistic values. The above procedure is performed iteratively

48   for 300 generations to reach the minimum of the cost function, which corresponds to the optimal

49   parameter set.

50   Previous parameter optimization studies have shown that it is difficult to constrain all model

51   parameters even for very simple ecosystem models because the information content of available

52   observations is typically insufficient (Matear, 1995; Fennel et al., 2001; Ward et al., 2010). Here we

53   conducted sensitivity tests to identify the parameters that are most sensitive to the available observations

54   and chose a subset of these to be optimized. In the **base case**, all parameters were at their initial guess

55   values obtained from the previous literature and some initial tuning. Then the **test cases** were run multiple

56   times by incrementally changing one parameter at a time to be the minimum, the first, second and third

57   quartile, and the maximum of its corresponding range while setting the other parameters to their initial

58   guess value (Table 1). The sensitivity was measured as the sum of a normalized absolute difference

59   between the base case (y_{Base}) and the test case (y_{Test})

60

61
$$Q(y, \vec{p}) = \frac{1}{m}\sum_{i=1}^{m}\frac{1}{n}\sum_{j=1}^{n}\frac{|y_{Base} - y_{Test}|}{y_{Base}} \qquad (6)$$

62

63 where m is the number of parameter increments (here 5) and n is the number of base-test pairs including

64 all 1D model grid cells throughout the whole simulation period for all variables to be compared.

65 Results of the sensitivity analysis are shown in Figure 2, where parameters are ranked by sensitivity

66 with respect to chlorophyll (Figure 2a) and the sum of chlorophyll, phytoplankton, and POC (Figure 2b).

67 POC is the sum of phytoplankton, zooplankton, and small and large detritus.

3.5. Parameter optimization experiments

69 For the parameter optimization of the 1D model, satellite chlorophyll within a 3×3 pixel (12 km×12

70 km area) around the 1D station and climatological monthly averages of the profiles from the bio-optical

71 floats were used.

72 To assess the effects of the optimization with respect to the different observation types, we conducted

73 three groups of experiments in which (A) surface satellite chlorophyll only, (B) surface satellite

74 chlorophyll and float profiles of chlorophyll, and (C) surface satellite chlorophyll and float profiles of

75 chlorophyll, phytoplankton, and POC were used. For each of these three groups, four to five optimizations

76 were conducted starting with the three most sensitive parameters and then adding one more parameter at

77 a time (Table 2) guided by the sensitivity analysis with respect to observed variables they used.

78 Specifically, groups A and B were based on the sensitivity analysis with respect to chlorophyll, while

79 group C was based on sensitivity analysis with respect to the sum of chlorophyll, phytoplankton, and

80 POC. Each optimization was replicated four times. The optimization with smallest model-data misfit

81 within each group was then used. Prior tests have shown that the available observations cannot

82 simultaneously constrain the sinking rates of small and large detritus (w_{SDet} and w_{LDet}). Therefore, a

83 constant ratio of 0.1 between these two parameters ($w_{SDet} = 0.1 \times w_{LDet}$) was imposed and only one of the

84 two was optimized. In groups A and B, the aggregation parameter τ was fixed at 0.05 because prior tests

85 generated unreasonably high values for this parameter.

86 We report two different metrics of misfits for these groups of experiments. The first metric, which

87 we refer to as the case-specific cost function value, is based on the optimized observations in a given

88 experiment and is minimized by the optimization algorithm, i.e.

89

$$F_A(\vec{p}) = F_{SurfCHL}(\vec{p}), \tag{8}$$

$$F_B(\vec{p}) = F_{SurfCHL}(\vec{p}) + F_{CHL}(\vec{p}), and \tag{9}$$

$$F_C(\vec{p}) = F_{SurfCHL}(\vec{p}) + F_{CHL}(\vec{p}) + F_{Phy}(\vec{p}) + F_{POC}(\vec{p}). \tag{10}$$

However, the models with lower case-specific misfit does not necessarily have better predictive skill in reproducing the unoptimized observations because of the so-called overfitting problem, e.g. the model may be tuned to reproduce optimized observations through wrong mechanisms (Friedrichs et al., 2006). To account for this, a second metric referred to as the total misfit is given by equ. 10. For group C, the second metric is the same as the case-specific cost function. For groups A and B, the total misfit metric allows us to assess improvements in the model's predictive skill to represent unoptimized fields.

4. Optimization of 1D models

4.1. Observations and base case

To provide context for the evaluation of our optimization experiments, the observations and the base case will be described first. As shown in Figure 3a, the observed surface chlorophyll shows a clear seasonality with the high concentrations in winter and low concentrations in summer. In the base case, the simulated surface chlorophyll fits observations well. Unlike the surface chlorophyll, the vertically integrated chlorophyll as well as the phytoplankton and POC over the upper 200 m tend to be more constant with much less seasonality (Figure 3b-d). This has been reported by Fommervault et al. (2017) who attributed the seasonality of surface chlorophyll to the vertical redistributions of subsurface chlorophyll and/or photoacclimation, rather than real changes in biomass.

The DCM is a ubiquitous phenomenon in the oligotrophic regions (Cullen, 2015). Observations detect a predominant DCM at around 60-100m depth throughout the whole year, with a sharp deepening in June and gradual shoaling after July (Figure 3e), reflecting the seasonality of the solar radiation. Unlike the large variability in the depth of the DCM, its magnitude is relatively constant at around 0.62 mg m^{-3} (Figure 3f). In the annually averaged profiles, the observed DCM is located at about 80 m depth with a

17 concentration of 0.52 mg m^{-3} (Figure 4a). The base case succeeds in reproducing the DCM at 65±7m

18 depth. However, it fails to reproduce the deepening of the DCM in June and the simulated annually

19 averaged depth of DCM is shallower by about 15 m than the observed. The simulated magnitude of the

20 DCM is about 2-fold larger than the observed (Figure 3f and Figure 4a) and hence the base case generally

21 overestimates vertically integrated chlorophyll (Figure 3b).

22   With respect to phytoplankton and POC, the observed maximum concentration occurs at about 60

23 m depth, which is 20 m above the DCM (Figure 4b-c). The observed vertical distributions of

24 phytoplankton and POC are not well captured by the base case. For example, phytoplankton and POC in

25 the upper layer are overestimated with the model-data discrepancies exceeding the variability of the

26 observations (Figure 4b-c). As a result, the base case yields an overall overestimation of the vertically

27 integrated phytoplankton and POC (Figure 3c-d).

28   Figure 4b also shows that both observed and simulated phytoplankton approach zero at about 160

29 m depth. Unlike phytoplankton, the observations show that the POC concentrations are 19 mg C m^{-3} at

30 about 200 m depth because of the existence of detritus (Figure 4c). However, the base case fails to

31 reproduce this non-zero POC concentrations, indicating that the model might be underestimating the

32 carbon export fluxes at 200 m.

33 **4.2. Results of the optimizations**

34 **4.2.1. Model-data misfits**

35   The case-specific cost function values and total misfits for the different 1D optimizations are shown

36 in Figure 5. Not surprisingly, all optimizations result in a reduction of the case-specific cost function

37 values. The extent of the reductions depends on the specific subset of parameters that were optimized.

38 However, the total misfits are not reduced in all optimizations. Optimizations A1 and A2 lead to slightly

39 larger total misfits than the base case and optimization B2 leads to a significantly larger total misfit. The

40 smallest total cost function values are achieved in A4, B4, and C4, i.e. in the experiments where a larger

41 subset of parameters was optimized (6 parameters). The optimal parameter sets (A4, B2, and C4), which

42 are selected based on case-specific misfit from these three groups, will be used in subsequent analyses

43   and hereafter are denoted simply as experiment A, experiment B, and experiment C. Further comparisons

44   are presented below to assess the impact of the different combinations of observations.

4.2.2. Experiment A

46   The optimal parameters from experiment A yield a 58% reduction in the misfit for surface

47   chlorophyll (Figure 5d). However, the vertical structure of chlorophyll deteriorates relative to the base

48   case (Figure 4a) because of inappropriate estimates of the initial slope (α=0.0101; see table 2) and the

49   maximum ratio of chlorophyll to carbon (θ_{max}=0.0191; see table 2). The annually averaged depth of the

50   DCM is lifted up to around 30±10m and the magnitude of DCM strongly decreases (Figure 3a, 4b).

51   Similar to chlorophyll, these deteriorations also manifest in the vertical phytoplankton and POC

52   distributions (Figure 4b-c). As a result, experiment A underestimates vertically integrated chlorophyll,

53   phytoplankton, and POC (Fig. 3b-d).

4.2.3. Experiment B

55   Due to the addition of observed chlorophyll profiles to the optimization in experiment B, the misfits

56   for surface and subsurface chlorophyll decrease relative to the base case (Figure 5d), but the reduction in

57   the misfit for surface chlorophyll (38%) is smaller than that in experiment A (58%). A straightforward

58   interpretation is that the addition of subsurface observations reduces the model's degrees of freedom to

59   fit one single observation type (surface chlorophyll). The vertical profile of chlorophyll is reproduced

60   better in experiment B than in the base case and experiment A in that the magnitude of the DCM is closer

61   to the observations, although the DCM depth is still too shallow, on average by about 20 m (Figure 4a).

62   The improvement in the vertical chlorophyll structure results in a better model-data fit of vertically

63   integrated chlorophyll (Figure 3b).

64   Despite the improvements in chlorophyll, the vertical profiles of phytoplankton and POC exhibit a

65   marked deterioration relative to the base case and experiment A (Figure 4b-c) because the parameter

66   optimization underestimates the maximum chlorophyll-to-carbon ratio (θ_{max} =0.0158; see table 2).

67   Experiment B leads to an overestimation of phytoplankton and POC relative to the base case with misfits

68   roughly 2.7 and 1.6 times larger than those of the base case, respectively (Figure 5d). Although

69   experiment B reproduces the non-zero POC concentrations at about 200 m depth, the proportion of

Biogeosciences
Discussions

70 phytoplankton in the POC pool is incorrect. In contrast to the observations where detritus dominates POC,

71 the simulated POC at 200 m is dominated by phytoplankton (49%) followed by zooplankton (39%).

72 **4.2.4. Experiment C**

73 Incorporating all observations (i.e. surface chlorophyll and profiles of chlorophyll, phytoplankton,

74 and POC) in experiment C improves the model-data misfits for almost all aspects except for surface

75 chlorophyll (Figure 3). Although a slight increase in the misfit occurs for the surface chlorophyll (~5%),

76 the total misfit is reduced by 75% compared to the base case. As shown in Figure 4a, the annually

77 averaged depth of DCM of 80 m coincides with the observed DCM, primarily because experiment C

78 reproduces the deepening of the DCM in summer. The magnitude of the DCM is also decreased relative

79 to the base case but remains higher than the observed. Phytoplankton and POC profiles exhibit only minor

80 deviations from the observations (Figure 4b-c). Importantly, experiment C reproduces the non-zero POC

81 concentrations at 200 m. In contrast to experiment B, phytoplankton in experiment C drops to zero at

82 about 160 m and POC is dominated by detritus (85%), which is more consistent with the observations.

83 **4.3. Simulated carbon fluxes**

84 Annually averaged carbon fluxes within the upper 200 m are shown for each experiment in Figure

85 6. The primary production in the base case amounts to 0.78 g C m^{-2} day^{-1}, of which 37% is consumed by

86 zooplankton, and the remaining 63% flows into detritus pools through sloppy feeding, mortality, and

87 aggregation of phytoplankton. As for the production of detritus, contributions from the phytoplankton

88 and zooplankton pools account for 70% and 30%, respectively. Most of the produced detritus is recycled

89 into the nutrient pool fueling recycled primary production, and only a small fraction is removed from the

90 upper layer through gravitational sinking. As a result, carbon export, which is estimated as the sum of

91 sinking fluxes by phytoplankton and detritus, is only 0.00032 g C m^{-2} day^{-1} and accounts for 0.04% of

92 primary production.

93 Due to the underestimation of phytoplankton in experiment A, primary production is reduced to 0.21

94 g C m^{-2} day^{-1} in that case. All other fluxes in the top 200 m decrease relative to the base case as well,

95 except for the export flux which increases to about 0.8% of primary production. This relative increase in

96 export is the result of larger sinking rates of phytoplankton and detritus (w_{Phy}=0.95, w_{LDet} =4.97; see table

15

97   2) than those used in the base case.

98   In contrast to experiment A, experiment B yields an increase of primary production relative to the
99   base case. The proportion of the grazing flux to primary production and the contribution of zooplankton
00   to the production of detritus also increase to about 59% and 52%, respectively. Unlike in the other three
01   experiments, carbon export in experiment B is dominated by the sinking of phytoplankton, reflecting its
02   large contribution to POC at 200 m. Although the simulated POC concentration at 200 m is very close to
03   the observations, the relative contributions of phytoplankton, zooplankton, and detritus are problematic
04   and likely do not result in a better estimation of carbon export (in this case 0.3% of primary production).

05   In experiment C, primary production is 0.30 g C m^{-2} day^{-1} with 24% flowing to zooplankton. The
06   mortality of zooplankton causes a flux of 0.047 g C m^{-2} day^{-1} to detritus, which accounts for 17% of the
07   production of detritus. Finally, about 24% of primary production is removed from the upper 200 m
08   through gravitational sinking. The simulated export ratio of 24% is within the wide range of reported
09   export ratios, from 6% to 43%, at 120 m depth in the Gulf of Mexico (see Table 3 of Hung et al., 2010).
10   Despite the high degree of uncertainty that exists when estimating export ratios (e.g., the global mean
11   export ratio varies from ~10% (Henson et al., 2012; Lima et al., 2014; Siegel et al., 2014) to ~20%
12   (Henson et al., 2015; Laws et al., 2000)), it is obvious that only experiment C reproduced an export ratio
13   of a reasonable magnitude. A more detailed validation of primary production and export fluxes will be
14   presented in the following sections.

15   **5.   3D biogeochemical model**

16   The optimal parameter sets from the 1D optimizations of A, B, and C were applied in the 3D model
17   for the whole GOM for five years (2011-2015). The performance of the 3D model can be regarded as a
18   cross-validation of the parameters optimized in 1D at different times and locations. It is possible that the
19   optimization algorithm has modified parameters to compensate for biases in the 1D simulations, e.g. the
20   absence of horizontal and vertical advection or the simplification of vertical diffusion, that degrades the
21   3D model performance. Indeed, directly applying the optimal parameter sets from 1D version to the 3D
22   model yields lower model-data agreement than the 1D counterpart and the following modifications to the
23   optimized parameters were made manually to bring the model-data agreement of 3D model in better

24   alignment with that of 1D version: the half-saturation for NH₄ uptake (k_{NH4}) was decreased to 0.01 in

25   experiment B and C, and the aggregation parameter (τ) was decreased to 0.05 in the experiment C.

26   **5.1. Spatial patterns of surface chlorophyll**

27   First, the annual climatological surface chlorophyll from satellite and model are compared from 2011

28   to 2015. The satellite estimates show high chlorophyll in the coastal regions and low chlorophyll in the

29   deep ocean (Figure 7a). This spatial pattern of surface chlorophyll is well reproduced in all simulations

30   except in the experiment A which even fails to reproduce the relatively high chlorophyll near the

31   Mississippi-Atchafalaya river systems because of the high sinking rate of phytoplankton (w_{Phy}=0.95; see

32   Table 2). The largest model-data differences occur in the coastal regions, where all simulations

33   underestimate the observed surface chlorophyll because parameter optimization is only performed at one

34   station located in the deep ocean without considering the coastal environments. Based on this and the fact

35   that the floats operated in the deep ocean (Figure 1), only the model results in the deep ocean (depth >

36   1000 m) will be considered in the following discussion.

37   **5.2. Subsurface distributions**

38   Figure 8 shows the seasonal cycles of surface chlorophyll as well as the vertically integrated

39   chlorophyll, phytoplankton, and POC within the deep ocean (depth>1000 m). Analogous to the 1D

40   models, chlorophyll, phytoplankton, and POC are integrated over the upper 200 m. Comparisons of

41   vertical profiles between observations and model results are given in Figure 9. In general, the main

42   features in the 3D models are very similar to those in 1D. Experiment A cannot constrain the vertical

43   profiles of chlorophyll because of the inappropriate estimation of initial slope (α), experiment B

44   overestimates phytoplankton and its contribution to POC since the maximum ratio of chlorophyll to

45   carbon (θ_{max}) is weakly constrained, and experiment C shows significant improvements in the model-data

46   agreement. However, there are some differences between the 1D and 3D models. For example, the base

47   case of the 1D model overestimates the magnitude while underestimating the depth of the observed DCM.

48   Experiment B and C best improve the magnitude and depth of DCM, respectively. In contrast, in the 3D

49   model the vertical profile of chlorophyll and the magnitude of the DCM in the base case are already very

50   close to the observations and neither of the optimizations yield further improvement. These differences

17

51   between the 1D and 3D models might be a result of different spatio-temporal scales between the two

52   model versions, or the simplifications of physical processes in the 1D model.

53   We have also compared the chlorophyll-to-carbon ratio, primary production, and carbon export

54   fluxes from 1D and 3D models with observations (Figure 10). The chlorophyll-to-carbon ratio is

55   estimated as the vertically integrated chlorophyll divided by the phytoplankton in the upper 200 m (Figure

56   10a). As an important indicator of phytoplankton physiological status (Geider, 1987), the observed

57   chlorophyll-to-carbon ratio varies considerably in response to the ambient environment. In general, the

58   ratios derived from the 3D models are lower than their corresponding 1D values, but the differences are

59   still within the range of variability. Without utilizing the observations of phytoplankton and POC,

60   experiments A and B in both 1D and 3D versions underestimate the chlorophyll-to-carbon ratio. In

61   experiment C, the simulated chlorophyll-to-carbon ratios from 1D and 3D are in good agreement with the

62   observations although the observed variability is underestimated.

63   For reference, satellite-based primary production (PP) is provided by two algorithms, the Vertically

64   Generalized Production Model (VGPM, Behrenfeld and Falkowski 1997) and the Carbon-based

65   Productivity Model (CbPM, Westberry et al. 2008). As shown in Figure 10b, satellite-based PP differs

66   depending on the algorithm applied. PP results from all 3D simulations are qualitatively similar to the 1D

67   simulations. Experiment C provides the best estimates of PP when compared to satellite-based estimates

68   from VGPM and CbPM, both in 1D and 3D.

69   The base case and experiments A and B yield carbon export fluxes smaller by one to two orders of

70   magnitude than experiment C. Thus, only experiment C from the 1D and 3D models are shown in Figure

71   10b in comparison to observations from sediment traps (see supplementary material). The carbon export

72   fluxes at 200 m from the 1D and 3D are similar in magnitude although the 1D model yields higher fluxes

73   and larger variability. Despite the scarcity of carbon export observations in the GOM, the model estimates

74   are within the range of observations down to ~1,600 m and capture the observed declining trend of carbon

75   export with depth.

76   In summary, all the results above demonstrate the feasibilities of using the locally optimized

77   parameters from the 1D model to improve the 3D simulation. In addition, by incorporating all available

78   observations (i.e. surface chlorophyll from satellite estimates, profiles of chlorophyll, phytoplankton, and

79   POC from bio-optical floats), experiment C cannot only simulate the biogeochemical processes well in

80   the upper 200 m, but also reproduce the carbon export flux and its associated attenuation in the deep ocean

81   (200-1600m) of the GOM.

82   **6.   Discussion**

83   **6.1.   Trade-offs between different observations for parameter optimization**

84   The results of the optimization experiments vary dramatically depending on how many observation

85   types are used. Using only satellite surface chlorophyll in experiment A succeeds in reducing the misfits

86   of surface chlorophyll, but at the expense of the vertical structure since the predominant DCM disappears

87   in experiment A. Satellite surface chlorophyll alone cannot constrain several vital parameters, including

88   the initial slope of the productivity-irradiance curve (α) and the maximum ratio of chlorophyll to carbon

89   (θ_{max}), with confidence. This result highlights the importance of subsurface observations for parameter

90   optimization and similarly for model validation.

91   The floats provide valuable subsurface observations, but chlorophyll profiles alone are not sufficient

92   for parameter optimization. In experiment B, the addition of chlorophyll profiles leads to significant

93   improvements in vertical chlorophyll distributions; however, the profiles of phytoplankton and POC

94   deteriorate largely because the maximum ratio of chlorophyll to carbon (θ_{max}) is weakly constrained.

95   Using estimates of phytoplankton biomass and POC derived from backscatter measurements in

96   experiment C yields the best estimation of plankton-related state variables and carbon fluxes (i.e. primary

97   production and carbon export). Only in this experiment do the improvements obtained from observations

98   in the upper 200 m extend to the deep ocean as reflected in the improved carbon export estimates below

99   1,000 m.

00   It should be noted, however, that degradation of unoptimized variables did not occur in all

01   optimizations within experiments A and B. In some cases, the unoptimized fields were improved. For

02   example, the A2 optimization yields a 69% reduction in the misfit for subsurface chlorophyll (Figure 5d)

03   and large improvements of chlorophyll profiles (Figure S5a) even though no observations of subsurface

04   chlorophyll are used. Another example is that B1 optimization improves simulations of phytoplankton

05 and POC (Figure 5d and Figure S5b-c) through the correlations between the observed chlorophyll and

06 phytoplankton ($r^2 = 0.69$) and POC ($r^2 = 0.69$). Similar findings have been reported in Prunet et al. (1996b)

07 where the improvements of chlorophyll profiles within the mixed layer were obtained by using surface

08 chlorophyll in a 1D model. In a more recent study by Xiao and Friedrichs (2014a) where satellite data

09 was used subsurface fields were improved in addition to surface fields.

10 In optimizations A2 and B1, the improvement in unoptimized fields occurred because the poorly

11 constrained parameters were not optimized but well defined ($\alpha = 0.125$ in the optimization A2 and $\theta_{max} =$

12 0.0535 in the optimization B1; see table 2). Including the unconstrained parameters into the parameter

13 optimization can return a lower misfit with respect to the observations used in optimization but increases

14 the risk of overfitting and reduces the model's predictive skill, i.e. the ability to simulate unoptimized

15 observations and those collected at different locations and times. This is consistent with previous studies

16 (Friedrichs et al., 2006, 2007; Ward et al., 2010). For example, Friedrichs et al. (2006) optimized three

17 ecosystem models of different complexities against three seasons of observations and the resulting

18 parameters were used to quantify the predictive skill for the fourth season. Cross-validation showed that

19 exclusion of the poorly constrained parameters from the optimization increased the predictive skill.

20 Although prior knowledge of the parameters allows one to exclude those poorly constrained ones

21 from the optimization and thus can prevent degradation in unoptimized variables, most parameters are

22 poorly known. Thus, the ultimate resolution of this issue should be to increase availability of observations

23 so that more parameters can be constrained with confidence. In addition, even if the unconstrained

24 parameters are well-known, a lack of observations hampers our ability to recognize improvements in the

25 model's predictive skill and hence may prevent us from identifying the optimal solutions. For example,

26 without the observations of phytoplankton and POC, we could not have known that optimization B1

27 improved simulations of phytoplankton and POC, let alone that the optimization B1 was a better solution

28 than the optimization B2 (the experiment B) in terms of the lower total misfit as shown in Figure 5d.

29 It has been suggested that when performing a parameter optimization, not only parameter values but

30 also parameter uncertainties should be taken into account (Fennel et al., 2001; Ward et al., 2010;

31 Bagniewski et al., 2011). The parameter uncertainties can be assessed by performing an uncertainty

32   analysis (Fennel et al., 2001; Prunet et al., 1996a, 1996b), replicating the parameter optimization (Ward

33   et al., 2010), and cross-validating the resulting parameters (Xiao and Friedrichs, 2014a). In this study, a

34   cross-validation of the parameters was conducted by evaluating the model's predictive skill with respect

35   to different variables, times, and locations. Although this cross-validation at different times and locations

36   may give some indication of overfitting, it cannot determine whether the model reproduces observations

37   through wrong mechanisms because a small misfit of cross-validation can be caused by missing

38   validations of key variables or fluxes, e.g. ignorance of phytoplankton and PP in the experiment B, while

39   a large misfit can be a result of the intrinsic heterogeneity of biological parameters in different times

40   (Mattern et al., 2012) and locations (Kidston et al., 2011), e.g. underestimation of coastal surface

41   chlorophyll in the experiment C. Therefore, it is important to evaluate the predictive skill of unoptimized

42   variables.

43   Collectively, the discussion above highlights the values of BGC float data for parameter optimization

44   and model validation, not only because of their high spatio-temporal coverage but also their ability to

45   measure multiple properties simultaneously.

6.2. Feasibilities of applying the local optimized parameters to 3D models

47   As the high computational cost makes direct optimization for a 3D biogeochemical model

48   impractical, we performed parameter optimizations first in a 1D surrogate model with the same

49   biogeochemical component as the 3D model. However, there are some difficulties in porting the locally

50   optimized parameters to the basin-scale model. Firstly, the 1D model necessarily neglects horizontal

51   advection, which can result in differences between the 1D and 3D models. On the one hand, the optimized

52   parameters from the 1D model may have been adjusted to compensate for biases in the biological

53   properties caused by neglecting advection and, as a result, this may degrade the 3D simulations (Kane et

54   al., 2011). On the other hand, counter examples exist where the 3D simulations outperform the 1D models

55   (Hoshiba et al., 2018). Secondly, the spatial heterogeneity of parameters (e.g., Kuhn and Fennel 2019) is

56   another issue that influences the portability of parameters from 1D to 3D models. In some studies, the

57   parameter optimization has been performed at several contrasting stations with the goal of using different

58   parameter sets in different regions of the 3D model (Hoshiba et al., 2018). In other studies different

59 stations were optimized simultaneously to obtain one single optimized parameter set (Kane et al., 2011;

60 Oschlies and Schartau, 2005; Schartau and Oschlies, 2003). Such parameters compromise the misfit in

61 each single station but take account into all stations and can often yield an overall better simulation of all

62 these stations as shown by Kuhn and Fennel (2019).

63   In our study, the similarities in general features between the 1D and 3D models confirm the

64 portability of the resulting parameters in the deep ocean of the GOM while the underestimation of surface

65 chlorophyll in the coastal regions may result from the contrasting ecosystem functioning between coastal

66 regions and deep ocean. For example, the highly productive continental shelf in the northern GOM is

67 fueled by the large nutrient load from the Mississippi and Atchafalaya river systems with primary

68 production being as high as 4 g C m^{-2} day^{-1} near the Mississippi river delta (Fennel et al., 2011), while

69 the deep ocean is oligotrophic and nutrient limited with the primary production ranging from 0.2 to 0.5 g

70 C m^{-2} day^{-1} (see Figure 10).

71 ## 7. Conclusions

72   In this study, we have performed parameter optimization for a 1D biogeochemical model and then

73 used the resulting parameters to generate simulations with a corresponding 3D model in the GOM. Three

74 experiments have been conducted by using different combinations of observations (surface chlorophyll

75 from satellite estimates, vertical profiles of chlorophyll, phytoplankton biomass and POC from BGC Argo

76 floats) in order to examine the trade-offs between the different observations for parameter optimization.

77 Two misfit metrics have been defined using the case-specific misfit and the total misfit to measure the

78 models' abilities to reproduce the optimized and unoptimized observations.

79   Model results show that satellite surface chlorophyll alone cannot reproduce well the vertical

80 structures in a biogeochemical model unless profile observations are used in addition. BGC Argo floats

81 are an excellent platform for obtaining such observations at high spatio-temporal coverage and for a

82 relatively broad suite of parameters. Only adding chlorophyll profiles is not sufficient because it fails to

83 constrain the ratio of chlorophyll to phytoplankton, but the addition of backscatter, which allows

84 estimation of phytoplankton biomass and POC, enables us to constrain the subsurface carbon state

85 variables and reproduce well PP and carbon export fluxes to below1000 m depth. Finally, our 3D model

86 was improved and reproduced similar results as the 1D version, which is promising for the application of

87 parameter optimization.

88

89 *Code and data availability:* The ROMS model code can be accessed at http://www.myroms.com (last

90 access: 16 June 2016). HYCOM data can be downloaded at http://tds.hycom.org/thredds/dodsC/datasets

91 (last access: 16 August 2018). Profiling data from the BGC-Argo floats are available at the National

92 Oceanographic Data Center (NOAA), https://data.nodc.noaa.gov/cgi-bin/iso?id=gov.noaa.nodc:159562

93 (Hamilton and Leidos, 2017)

94

95 *Author contributions.* BW and KF conceived the study. BW carried out optimization experiments, model

96 simulations and analyses. LY assisted with set-up and validation of the 3D model. CG assisted with

97 processing of the BGC float data. BW and KF discussed the results and wrote the paper with contributions

98 from the coauthors.

99

00 *Competing interests.* The authors declare that they have no conflict of interest.

01

02 *Financial support.* This research was funded by the Gulf of Mexico Research Initiative (GoMRI-V-487).

03

04

05

06

07

08

09

10

References

11   Bagniewski, W., Fennel, K., Perry, M. J. and D'Asaro, E. A.: Optimizing models of the North Atlantic spring bloom using physical, chemical and bio-optical observations from a Lagrangian float, Biogeosciences, 8, 1291–1307, doi:10.5194/bg-8-1291-2011, 2011.

Behrenfeld, M. J. and Falkowski, P. G.: Photosynthetic rates derived from satellite-based chlorophyll concentration, Limnology and Oceanography, 42(1), 1–20, 1997.

Behrenfeld, M. J., Boss, E., Siegel, D. A. and Shea, D. M.: Carbon-based ocean productivity and phytoplankton physiology from space, Global Biogeochemical Cycles, 19(1), 1–14, doi:10.1029/2004GB002299, 2005.

Biogeochemical-Argo Planning Group: The scientific rationale, design and implementation plan for a Biogeochemical-Argo float array, edited by Ken Johnson and Hervé Claustre., 2016.

Boss, E. B. and Haëntjens, N.: Primer regarding measurements of chlorophyll fluorescence and the backscattering coefficient with WETLabs FLBB on profiling floats., 2016.

Briggs, N., Perry, M. J., Cetinic´, I., Lee, C., D'Asaro, E., Gray, A. M. and Rehm, E.: High-resolution observations of aggregate flux during a sub-polar North Atlantic spring bloom, Deep-Sea Research I, 58, 1031–1039, doi:10.1016/j.dsr.2011.07.007, 2011.

Cullen, J. J.: Subsurface Chlorophyll Maximum Layers : Enduring Enigma or Mystery Solved ?, Annual Review of Marine Science, 7, 207–239, doi:10.1146/annurev-marine-010213-135111, 2015.

Denman, K. L.: Modelling planktonic ecosystems : parameterizing complexity, Progress in Oceanography, 57, 429–452, doi:10.1016/S0079-6611(03)00109-5, 2003.

Doney, S. C., Lima, I., Moore, J. K., Lindsay, K., Behrenfeld, M. J., Westberry, T. K., Mahowald, N., Glover, D. M. and Takahashi, T.: Skill metrics for confronting global upper ocean ecosystem-biogeochemistry models against field and remote sensing data, Journal of Marine Systems, 76, 95–112, doi:10.1016/j.jmarsys.2008.05.015, 2009.

Fennel, K. and Boss, E.: Subsurface maxima of phytoplankton and chlorophyll : Steady-state solutions from a simple model, Limnology and Oceanography, 48(4), 1521–1534, 2003.

Fennel, K., Losch, M., Schroter, J. and Wenzel, M.: Testing a marine ecosystem model : sensitivity

38   analysis and parameter optimization, Journal of Marine Systems, 28, 45–63, 2001.

39   Fennel, K., Wilkin, J., Levin, J., Moisan, J., Reilly, J. O. and Haidvogel, D.: Nitrogen cycling in the

40   Middle Atlantic Bight : Results from a three-dimensional model and implications for the North

41   Atlantic   nitrogen   budget,   GLOBAL   BIOGEOCHEMICAL   CYCLES,   20,   1–14,

42   doi:10.1029/2005GB002456, 2006.

43   Fennel, K., Hetland, R., Feng, Y. and Dimarco, S.: A coupled physical-biological model of the Northern

44   Gulf of Mexico shelf: Model description, validation and analysis of phytoplankton variability,

45   Biogeosciences, 8, 1881–1899, doi:10.5194/bg-8-1881-2011, 2011.

46   Fommervault, O. P. De, Perez-brunius, P., Damien, P., Camacho-ibar, V. F. and Sheinbaum, J.: Temporal

47   variability of chlorophyll distribution in the Gulf of Mexico: bio-optical data from profiling floats,

48   Biogeosciences, 14, 5647–5662, doi:10.5194/bg-14-5647-2017, 2017.

49   Friedrichs, M. A. M., Hood, R. R. and Wiggert, J. D.: Ecosystem model complexity versus physical

50   forcing: Quantification of their relative impact with assimilated Arabian Sea data, Deep-Sea Research

51   Part II, 53, 576–600, doi:10.1016/j.dsr2.2006.01.026, 2006.

52   Friedrichs, M. A. M., Dusenberry, J. A., Anderson, L. A., Armstrong, R. A., Chai, F., Christian, J. R.,

53   Doney, S. C., Dunne, J., Fujii, M., Hood, R., Jr, D. J. M., Moore, J. K., Schartau, M., Spitz, Y. H.

54   and Wiggert, J. D.: Assessment of skill and portability in regional marine biogeochemical models:

55   Role   of   multiple   planktonic   groups,   Journal   of   Geophysical   Research,   112,   1–22,

56   doi:10.1029/2006JC003852, 2007.

57   Geider, R. J.: Light and temperature dependence of the carbon to chlorophyll a ratio in microalgae and

58   cyanobacteria: implications for physiology and growth of phytoplankton, New Phytologist, 106, 1–

59   34, 1987.

60   Geider, R. J., MacIntyre, H. L. and Kana, T. M.: Dynamic model of phytoplankton growth and

61   acclimation : responses of the balanced growth rate and the chlorophyll a : carbon ratio to light ,

62   nutrient-limitation and temperature, Marine ecology progress series, 148, 187–200, 1997.

63   Gomez, F. A., Lee, S., Liu, Y., Jr, F. J. H., Muller-karger, F. E. and Lanmkin, J. T.: Seasonal patterns in

64   phytoplankton biomass across the northern and deep Gulf of Mexico : a numerical model study,

65   Biogeosciencesg, 15, 3561–3576, doi:10.5194/bg-15-3561-2018, 2018.

66 Green, R. E., Bower, A. S. and Lugo-Fernandez, A.: First Autonomous Bio-Optical Profiling Float in the

67   Gulf of Mexico Reveals Dynamic Biogeochemistry in Deep Waters, PLoS ONE, 9(7), 1–9,

68   doi:10.1371/journal.pone.0101658, 2014.

69 Haidvogel, D. B., Arango, H., Budgell, W. P., Cornuelle, B. D., Curchitser, E., Lorenzo, E. Di, Fennel,

70   K., Geyer, W. R., Hermann, A. J., Lanerolle, L., Levin, J., McWilliams, J. C., Miller, A. J., Moore,

71   A. M., Powell, T. M., Shchepetkin, A. F., Sherwood, C. R., Signell, R. P., Warner, J. C. and Wilkin,

72   J.: Ocean forecasting in terrain-following coordinates : Formulation and skill assessment of the

73   Regional Ocean Modeling System, Journal of computational physics, 227, 3595–3624,

74   doi:10.1016/j.jcp.2007.06.016, 2008.

75 Hamilton, P. and Leidos: Ocean currents, temperatures, and others measured by drifters and profiling

76   floats for the Lagrangian Approach to Study the Gulf of Mexico Deep Circulation project 2011-07

77   to 2015-06 (NCEI Accession 0159562), Version 1.1, NOAA National Centers for Environmental

78   Information. Dataset, available at https://accession.nodc.noaa.gov/0159562, last access: 25 October

79   2017.

80 Henson, S. A., Sanders, R. and Madsen, E.: Global patterns in efficiency of particulate organic carbon

81   export   and   transfer   to   the   deep   ocean,   Global   Biogeochemical   Cycles,   26(1),

82   doi:10.1029/2011GB004099, 2012.

83 Henson, S. A., Yool, A. and Sanders, R.: Variability in efficiency of particulate organic carbon export: A

84   model study, Global Biogeochemical Cycles, 29(1), 33–45, doi:10.1002/2014GB004965, 2015.

85 Hoshiba, Y., Hirata, T., Shigemitsu, M., Nakano, H., Hashioka, T., Masuda, Y. and Yamanaka, Y.:

86   Biological data assimilation for parameter estimation of a phytoplankton functional type model for

87   the western North Pacific, Ocean Science, 14, 371–386, doi:10.5194/os-14-371-2018, 2018.

88 Hung, C.-C., Xu, C., Santschi, P. H., Zhang, S.-J., Schwehr, K. A., Quigg, A., Guo, L., Gong, G.-C.,

89   Pinckney, J. L., Long, R. A. and Wei, C.-L.: Comparative evaluation of sediment trap and 234Th-

90   derived POC fluxes from the upper oligotrophic waters of the Gulf of Mexico and the subtropical

91   northwestern   Pacific   Ocean,   Marine   Chemistry,   121(1),   132–144,

92   doi:https://doi.org/10.1016/j.marchem.2010.03.011, 2010.

93   Kane, A., Moulin, C., Thiria, S., Bopp, L., Berrada, M., Tagliabue, A., Crépon, M., Aumont, O. and

94   Badran, F.: Improving the parameters of a global ocean biogeochemical model via variational

95   assimilation of in situ data at five time series stations, Journal of Geophysical Research: Oceans, 116,

96   1–14, doi:10.1029/2009JC006005, 2011.

97   Kidston, M., Matear, R. and Baird, M. E.: Parameter optimisation of a marine ecosystem model at two

98   contrasting stations in the Sub-Antarctic Zone, Deep-Sea Research II, 58, 2301–2315,

99   doi:10.1016/j.dsr2.2011.05.018, 2011.

00   Kuhn, A. M. and Fennel, K.: Evaluating ecosystem model complexity for the northwest North Atlantic

01   through   surrogate-based   optimization,   Ocean   Modelling,   142,   101437,

02   doi:https://doi.org/10.1016/j.ocemod.2019.101437, 2019.

03   Kuhn, A. M., Fennel, K. and Mattern, J. P.: Progress in Oceanography Model investigations of the North

04   Atlantic   spring   bloom   initiation,   Progress   in   Oceanography,   138,   176–193,

05   doi:10.1016/j.pocean.2015.07.004, 2015.

06   Kuhn, A. M., Fennel, K. and Berman-frank, I.: Modelling the biogeochemical effects of heterotrophic

07   and autotrophic N2 fixation in the Gulf of Aqaba (Israel), Red Sea, Biogeosciences, 15, 7379–7401,

08   doi:10.5194/bg-15-7379-2018, 2018.

09   Lagman, K. B., Fennel, K., Thompson, K. R. and Bianucci, L.: Assessing the utility of frequency

10   dependent nudging for reducing biases in biogeochemical models, Ocean Modelling, 81, 25–35,

11   doi:https://doi.org/10.1016/j.ocemod.2014.06.006, 2014.

12   Laurent, A., Fennel, K., Cai, W. J., Huang, W. J., Barbero, L. and Wanninkhof, R.: Eutrophication-

13   induced acidification of coastal waters in the northern Gulf of Mexico: Insights into origin and

14   processes from a coupled physical-biogeochemical model, Geophysical Research Letters, 44(2),

15   946–956, doi:10.1002/2016GL071881, 2017.

16   Laws, E. A., Falkowski, P. G., Smith Jr., W. O., Ducklow, H. and McCarthy, J. J.: Temperature effects

17   on export production in the open ocean, Global Biogeochemical Cycles, 14(4), 1231–1246,

18   doi:10.1029/1999GB001229, 2000.

19 Lehmann, M. K., Fennel, K. and He, R.: Statistical validation of a 3-D bio-physical model of the western
20   North Atlantic, Biogeosciences, 6(10), 1961–1974, doi:10.5194/bg-6-1961-2009, 2009.

21 Lima, I. D., Lam, P. J. and Doney, S. C.: Dynamics of particulate organic carbon flux in a global ocean
22   model, Biogeosciences, 11(4), 1177–1198, doi:10.5194/bg-11-1177-2014, 2014.

23 Martínez-López, B. and Zavala-Hidalgo, J.: Seasonal and interannual variability of cross-shelf transports
24   of chlorophyll in the Gulf of Mexico, Journal of Marine Systems, 77, 1–20,
25   doi:10.1016/j.jmarsys.2008.10.002, 2009.

26 Martinez-Vicente, V., Dall'Olmo, G., Tarran, G., Boss, E. and Sathyendranath, S.: Optical backscattering
27   is correlated with phytoplankton carbon across the Atlantic Ocean, Geophysical Research Letters,
28   40, 1154–1158, doi:10.1002/grl.50252, 2013.

29 Matear, R. J.: Parameter optimization and analysis of ecosystem models using simulated annealing : A
30   case study at Station P, Journal of Marine Research, 53, 571–607, 1995.

31 Mattern, J. P. and Edwards, C. A.: Simple parameter estimation for complex models — Testing
32   evolutionary techniques on 3-dimensional biogeochemical ocean models, Journal of Marine Systems,
33   165, 139–152, doi:10.1016/j.jmarsys.2016.10.012, 2017.

34 Mattern, J. P., Fennel, K. and Dowd, M.: Estimating time-dependent parameters for a biological ocean
35   model using an emulator approach, Journal of Marine Systems, 96–97, 32–47,
36   doi:https://doi.org/10.1016/j.jmarsys.2012.01.015, 2012.

37 Mellor, G. L. and Yamada, T.: Development of a turbulence closure model for geophysical fluid
38   problems, Reviews of Geophysics and Space Physics, 20(4), 851–875,
39   doi:10.1029/RG020i004p00851, 1982.

40 Mignot, A., Claustre, H., Uitz, J., Poteau, A., D'Ortenzio, F. and Xing, X.: Understanding the seasonal
41   dynamics of phytoplankton biomass and the deep chlorophyll maximum in oligotrophic
42   environments: A Bio-Argo float investigation, Global Biogeochemical Cycles, 28(8), 1–21,
43   doi:10.1002/2013GB004781, 2014.

44 Muller-Karger, F. E., Walsh, J. J., Evans, R. H. and Meyers, M. B.: On the Seasonal Phytoplankton
45   Concentration and Sea Surface Temperature Cycles of the Gulf of Mexico as Determined by

46   Satellites, Journal of Geophysical Research, 96, 12645–12665, 1991.

47   Muller-Karger, F. E., Smith, J. P., Werner, S., Chen, R., Roffer, M., Liu, Y., Muhling, B., Lindo-atichati,
48   D., Lamkin, J., Cerdeira-estrada, S. and Enfield, D. B.: Natural variability of surface oceanographic
49   conditions in the offshore Gulf of Mexico, Progress in Oceanography, 134, 54–76,
50   doi:10.1016/j.pocean.2014.12.007, 2015.

51   Oschlies, A. and Schartau, M.: Basin-scale performance of a locally optimized marine ecosystem model,
52   Journal of Marine Research, 63(2), 335–358, 2005.

53   Prunet, P., Minster, J., Ruiz-Pino, D. and Dadou, I.: Assimilation of surface data in a one-dimensional
54   physical-biogeochemical model of the surface ocean 1 . Method and preliminary results, GLOBAL
55   BIOGEOCHEMICAL CYCLES, 10(1), 111–138, 1996a.

56   Prunet, P., Minster, J., Echevin, V. and Dadou, I.: Assimilation of surface data in a one-dimensional
57   physical-biogeochemical model of the surface ocean 2. Ajusting a simple trophic model to
58   chlorophyll, temperature, nitrate, and pCO2 data, GLOBAL BIOGEOCHEMICAL CYCLES, 10(1),
59   139–158, 1996b.

60   Rasse, R., Dall'Olmo, G., Graff, J., Westberry, T. K., van Dongen-Vogels, V. and Behrenfeld, M. J.:
61   Evaluating Optical Proxies of Particulate Organic Carbon across the Surface Atlantic Ocean,
62   Frontiers in Marine Science, 4(November), 1–18, doi:10.3389/fmars.2017.00367, 2017.

63   Roemmich, D., Alford, M. H., Claustre, H., Johnson, K., King, B., Moum, J., Oke, P., Owens, W. B.,
64   Pouliquen, S., Purkey, S., Scanderbeg, M., Suga, T., Wijffels, S., Zilberman, N., Bakker, D.,
65   Baringer, M., Belbeoch, M., Bittig, H. C., Boss, E., Calil, P., Carse, F., Carval, T., Chai, F.,
66   Conchubhair, D. Ó., D'Ortenzio, F., Dall'Olmo, G., Desbruyeres, D., Fennel, K., Fer, I., Ferrari, R.,
67   Forget, G., Freeland, H., Fujiki, T., Gehlen, M., Greenan, B., Hallberg, R., Hibiya, T., Hosoda, S.,
68   Jayne, S., Jochum, M., Johnson, G. C., Kang, K., Kolodziejczyk, N., Körtzinger, A., Traon, P.-Y. Le,
69   Lenn, Y.-D., Maze, G., Mork, K. A., Morris, T., Nagai, T., Nash, J., Garabato, A. N., Olsen, A.,
70   Pattabhi, R. R., Prakash, S., Riser, S., Schmechtig, C., Schmid, C., Shroyer, E., Sterl, A., Sutton, P.,
71   Talley, L., Tanhua, T., Thierry, V., Thomalla, S., Toole, J., Troisi, A., Trull, T. W., Turton, J., Velez-
72   Belchi, P. J., Walczowski, W., Wang, H., Wanninkhof, R., Waterhouse, A. F., Waterman, S., Watson,

73   A., Wilson, C., Wong, A. P. S., Xu, J. and Yasuda, I.: On the Future of Argo: A Global, Full-Depth,
74   Multi-Disciplinary Array, Frontiers in Marine Science, 6, 439 [online] Available from:
75   https://www.frontiersin.org/article/10.3389/fmars.2019.00439, 2019.

76   Schartau, M. and Oschlies, A.: Simultaneous data-based optimization of a 1D-ecosystem model at three
77   locations in the North Atlantic : Part I — Method and parameter estimates, Journal of Marine
78   Research, 61, 765–793, 2003.

79   Shchepetkin, A. F. and Mcwilliams, J. C.: The regional oceanic modeling system (ROMS): a split-
80   explicit, free-surface, topography-following-coordinate oceanic model, Ocean Modelling, 9, 347–
81   404, doi:10.1016/j.ocemod.2004.08.002, 2005.

82   Siegel, D. A., Buesseler, K. O., Doney, S. C., Sailley, S. F., Behrenfeld, M. J. and Boyd, P. W.: Global
83   assessment of ocean carbon export by combining satellite observations and food-web models, Global
84   Biogeochemical Cycles, 28(3), 181–196, doi:10.1002/2013GB004743, 2014.

85   Smagorinsky, J.: General circulation experiments with the primitive equations: I. the basic experiment,
86   Monthly Weather Review, 91(3), 99–164, 1963.

87   Smolarkiewicz, P. K. and Margolin, L. G.: MPDATA : A Finite-Difference Solver for Geophysical
88   Flows, Journal of computational physics, 140, 459–480, 1998.

89   Tjiputra, J. F., Polzin, D. and Winguth, A. M. E.: Assimilation of seasonal chlorophyll and nutrient data
90   into an adjoint three-dimensional ocean carbon cycle model : Sensitivity analysis and ecosystem
91   parameter optimization, Global Biogeochemical Cycles, 21, 1–13, doi:10.1029/2006GB002745,
92   2007.

93   Ward, B. A., Friedrichs, M. A. M., Anderson, T. R. and Oschlies, A.: Parameter optimisation techniques
94   and the problem of underdetermination in marine biogeochemical models, Journal of Marine
95   Systems, 81, 34–43, doi:10.1016/j.jmarsys.2009.12.005, 2010.

96   Westberry, T., Behrenfeld, M. J., Siegel, D. A. and Boss, E.: Carbon-based primary productivity modeling
97   with vertically resolved photoacclimation, GLOBAL BIOGEOCHEMICAL CYCLES, 22, 1–18,
98   doi:10.1029/2007GB003078, 2008.

99   Xiao, Y. and Friedrichs, M. A. M.: The assimilation of satellite-derived data into a one-dimensional lower

00   trophic level marine ecosystem model, Journal of Geophysical Research: Oceans, 119, 2691–2712,

01   doi:10.1002/2013JC009433.Received, 2014a.

02   Xiao, Y. and Friedrichs, M. A. M.: Using biogeochemical data assimilation to assess the relative skill of

03   multiple ecosystem models in the Mid-Atlantic Bight : effects of increasing the complexity of the

04   planktonic food web, Biogeosciences, 11, 3015–3030, doi:10.5194/bg-11-3015-2014, 2014b.

05   Xue, Z., He, R., Fennel, K., Cai, W., Lohrenz, S. and Hopkinson, C.: Modeling ocean circulation and

06   biogeochemical variability in the Gulf of Mexico, Biogeosciences, 10, 7219–7234, doi:10.5194/bg-

07   10-7219-2013, 2013.

08   Yu, L., Fennel, K. and Laurent, A.: A modeling study of physical controls on hypoxia generation in the

09   northern Gulf of Mexico, Journal of Geophysical Research: Oceans, 120(7), 5019–5039,

10   doi:10.1002/2014JC010634, 2015.

11

12

13

14

15

16

17

18

19

20

21

22

23

24

25

26

27

28

Table list

Table 1. Initial values and ranges of primary parameters used in the biogeochemical model

Descriptions (unit)	Symbol	Value	Range
Radiation threshold for nitrification (W m^{-2})	I_0	0.0095[a]	0.005[b]-0.01[b]
Half-saturation radiation for nitrification (W m^{-2})	k_I	0.1[a]	0.01[b]-0.5[b]
Maximum nitrification rate (day^{-1})	n_{max}	0.2[c]	0.01[b]-0.35[b]
Phytoplankton growth at 0 °C (Dimensionless)	μ_0	0.69[a]	0.1[b]-3.0[b]
Initial slope of P-I curve (mg_C (mg_Chl W m^{-2} day)$^{-1}$)	α	0.125[a]	0.007[a]-0.13[a]
Half-saturation for NO$_3$ uptake (mmol_N m^{-3})	k_{NO3}	0.5[a]	0.007[a]-1.5[a]
Half-saturation for NH$_4$ uptake (mmol_N m^{-3})	k_{NH4}	0.5[a]	0.007[a]-1.5[a]
Phytoplankton mortality (day^{-1})	m_P	0.075	0.01[b]-0.2[b]
Aggregation parameter (day^{-1})	τ	0.1	0.01[b]-25[b]
Maximum chlorophyll to carbon ratio (mg_Chl mg_C^{-1})	θ_{max}	0.0535[c]	0.005[a]-0.15[b]
Phytoplankton sinking velocity (m day^{-1})	w_{Phy}	0.1[a]	0.009[a]-25[a]
Maximum grazing rate (day^{-1})	g_{max}	0.6[a]	0.1[b]-4[b]
Half-saturation for phytoplankton ingestion ((mmol_N m^{-3})^2)	k_P	0.5	0.01[b]-3.5[a]
Zooplankton assimilation efficiency (Dimensionless)	β	0.75[a]	0.25[b]-0.75[b]
Zooplankton basal metabolism (day^{-1})	l_{BM}	0.01	0.01[b]-0.15[b]
Zooplankton specific excretion (day^{-1})	l_E	0.1[a]	0.05[b]-0.35[b]
Zooplankton mortality (day^{-1})	m_Z	0.2	0.02[b]-0.35[b]
Small detritus remineralization (day^{-1})	r_{SD}	0.3[c]	0.005[b]-0.25[a]
Large detritus remineralization (day^{-1})	r_{LD}	0.1	0.005[b]-0.25[a]
Small detritus sinking velocity (m day^{-1})	w_{SDet}	0.1[a]	0.009[a]-25[a]
Large detritus sinking velocity (m day^{-1})	w_{LDet}	1[a]	0.009[a]-25[a]

a Fennel et al. (2006); b Kuhn et al. (2018); c Yu et al. (2015)

Biogeosciences
Discussions

32

33

34 Table 2. The best fit of parameter set for each experiment

	w_{Phy}	m_P	k_{NH4}	τ	θ_{max}	α	w_{LDet}
Base	0.1000	0.0750	0.5000	0.1000	0.0535	0.1250	1.000
A1	0.0608	0.0100	1.5000	--	--	--	--
A2	0.6863	0.0100	0.0195	--	0.0169	--	--
A3	1.6567	0.1978	0.1004	--	0.0250	0.0219	--
A4	0.9468	0.0737	0.2454	--	0.0191	0.0101	4.9694
B1	0.2863	0.0983	1.5000	--	--	--	--
B2	0.4217	0.0130	0.0300	--	0.0158	--	--
B3	2.1016	0.0176	1.5000	--	0.0346	0.0079	--
B4	0.0090	0.0100	1.5000	--	0.0361	0.0405	8.3514

	w_{Phy}	r_{LD}	m_P	τ	k_{NH4}	w_{LDet}	θ_{max}
Base	0.1000	0.1000	0.0750	0.1000	0.5000	1.0000	0.0535
C1	1.9231	0.2500	0.1805	--	--	--	--
C2	0.9755	0.2500	0.0100	1.1402	--	--	--
C3	0.4071	0.0630	0.0100	1.8531	0.0070	--	--
C4	0.0090	0.0050	0.0634	0.0995	0.0431	5.6623	--
C5	0.0090	0.2245	0.0100	0.6451	1.5000	2.5202	0.0614

35

36

37

38

39

40

41

42

43

Figure captions

45

46
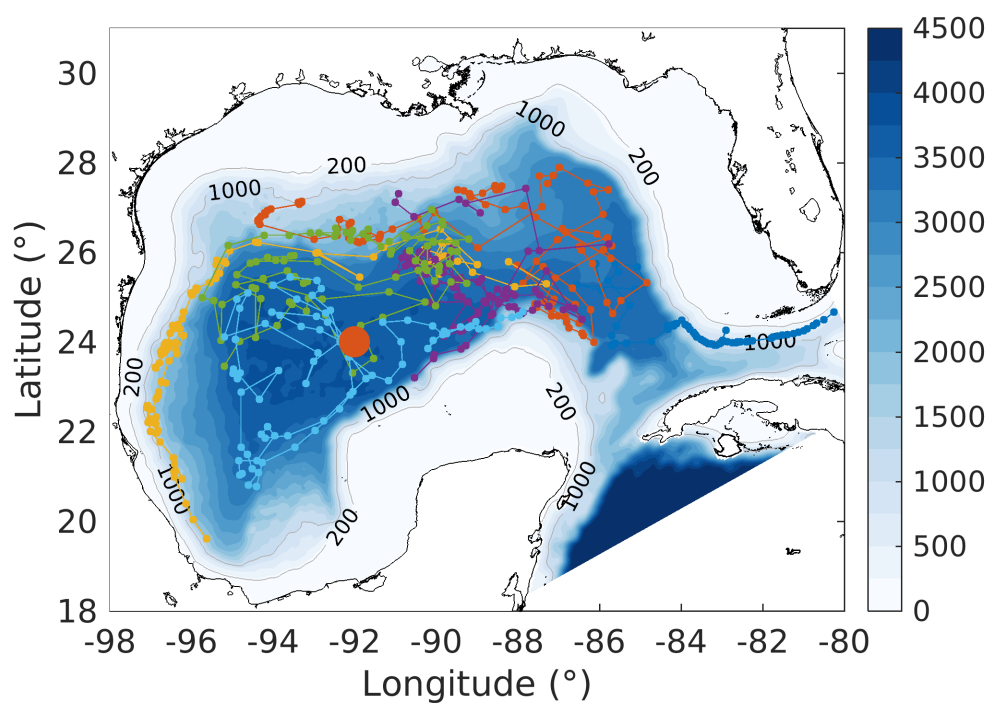
Figure 1. Model bathymetry (unit: m) with trajectories of six bio-optical floats (small colored dots and lines) which operated in the Gulf of Mexico from 2011 to 2015. The location of the 1D model is denoted by the large orange dot.
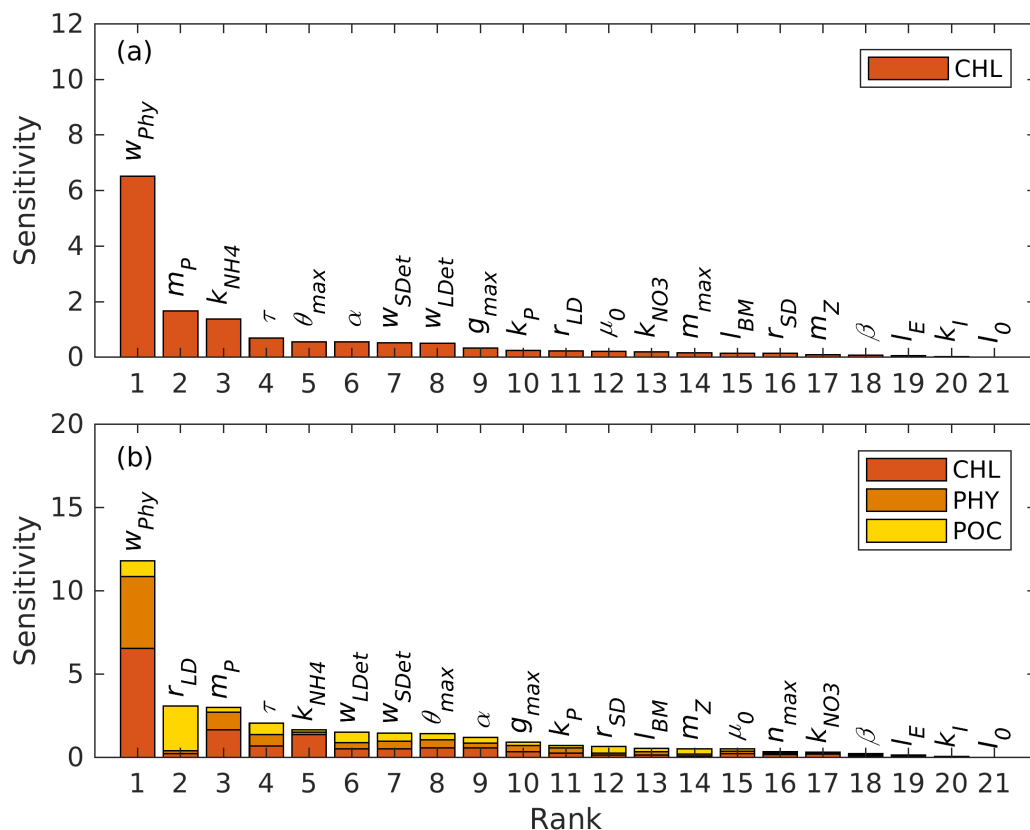
Figure 2. Parameter sensitivities (unit: dimensionless) with respect to (a) chlorophyll and (b) the sum of chlorophyll, phytoplankton, and POC.
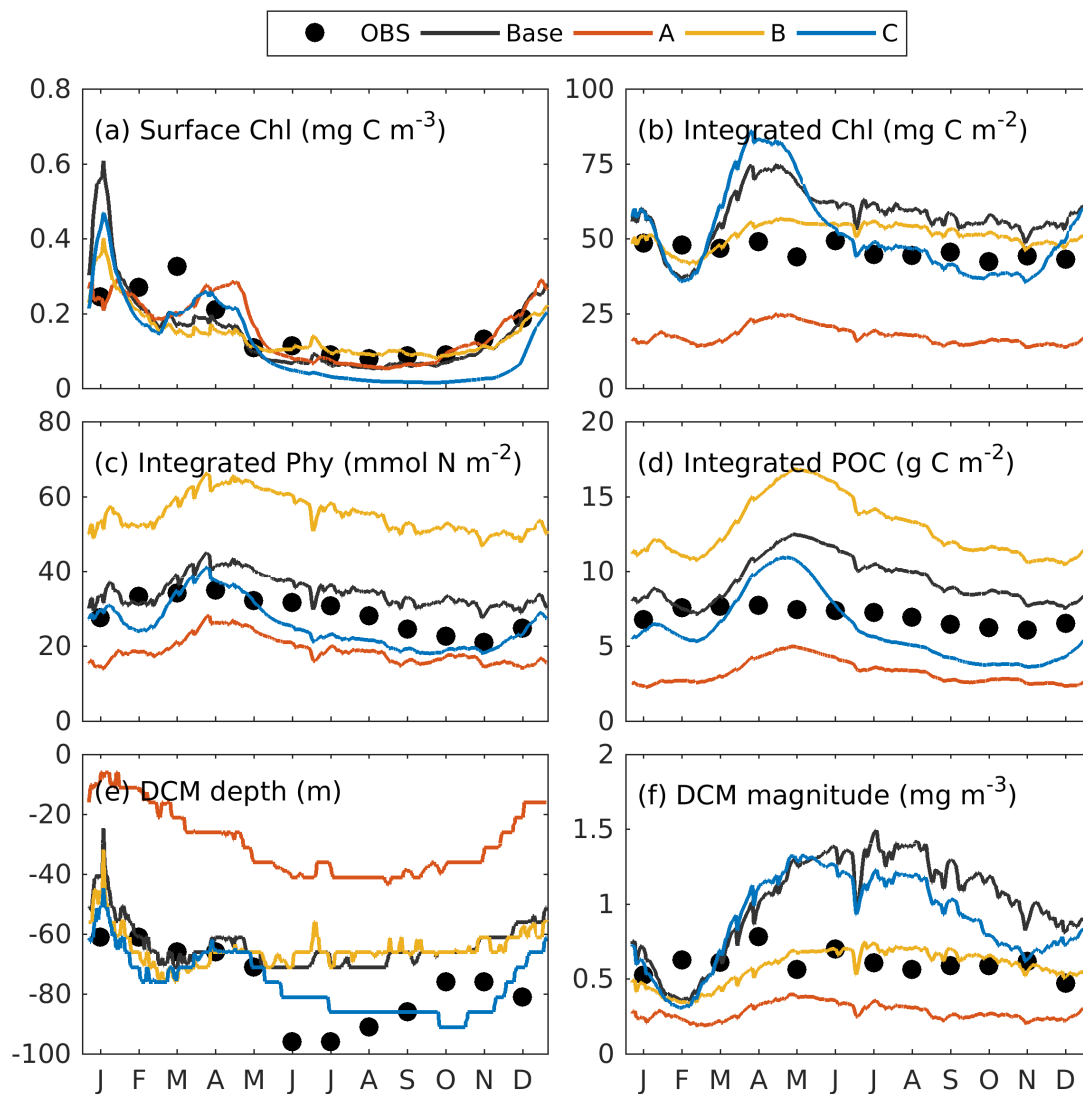
Figure 3. Observed (black dots) and simulated (colored lines) annual cycle of surface chlorophyll (a), vertically integrated chlorophyll (b), vertically integrated phytoplankton (c), vertically integrated POC (d), and the depth (e) and magnitude (f) of the DCM. Chlorophyll, phytoplankton, zooplankton, and POC are integrated over the top 200 m.
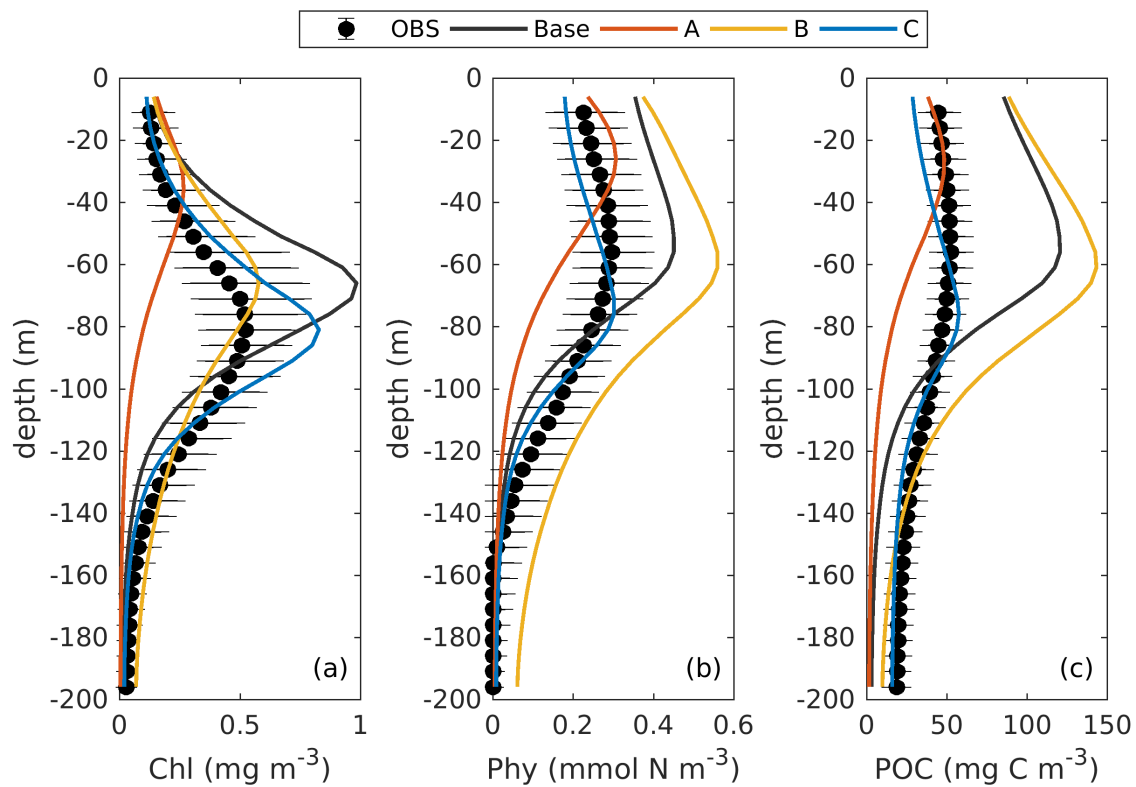
Figure 4. Observed (black dots with error bars) and simulated (colored lines) vertical profiles of chlorophyll, phytoplankton, and POC.
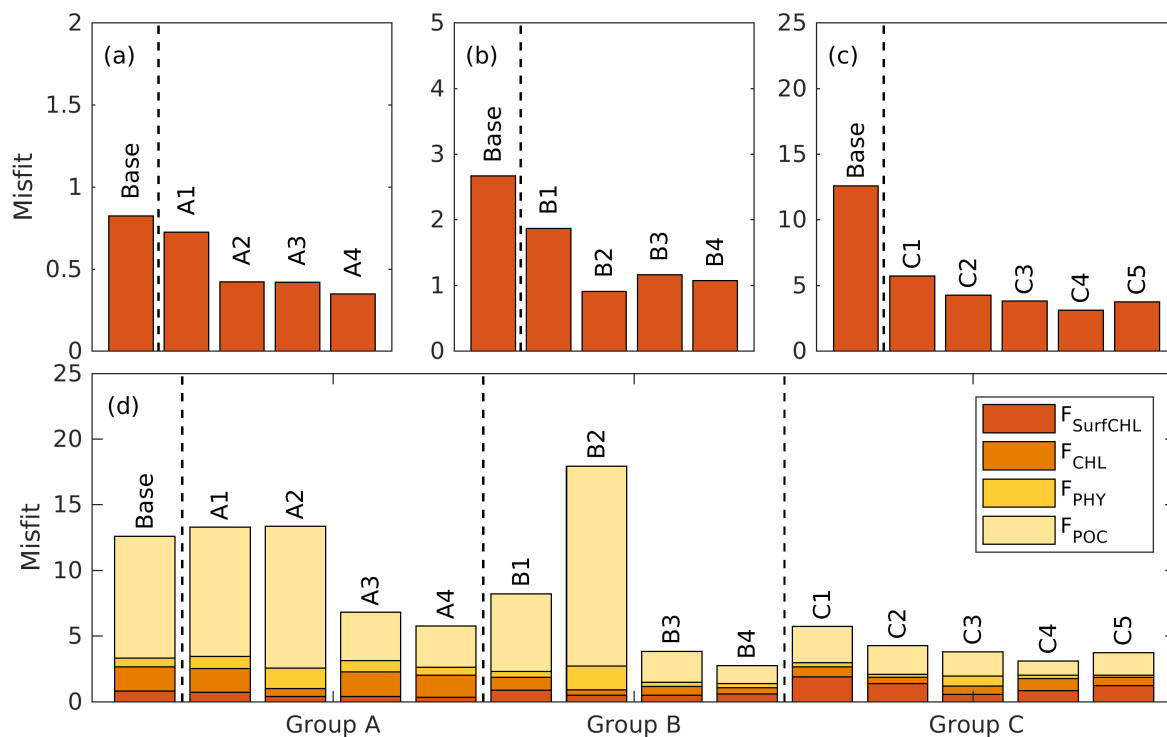
Figure 5. The case-specific cost function values (a-c) and total misfits (d) of the base case and the different optimizations.
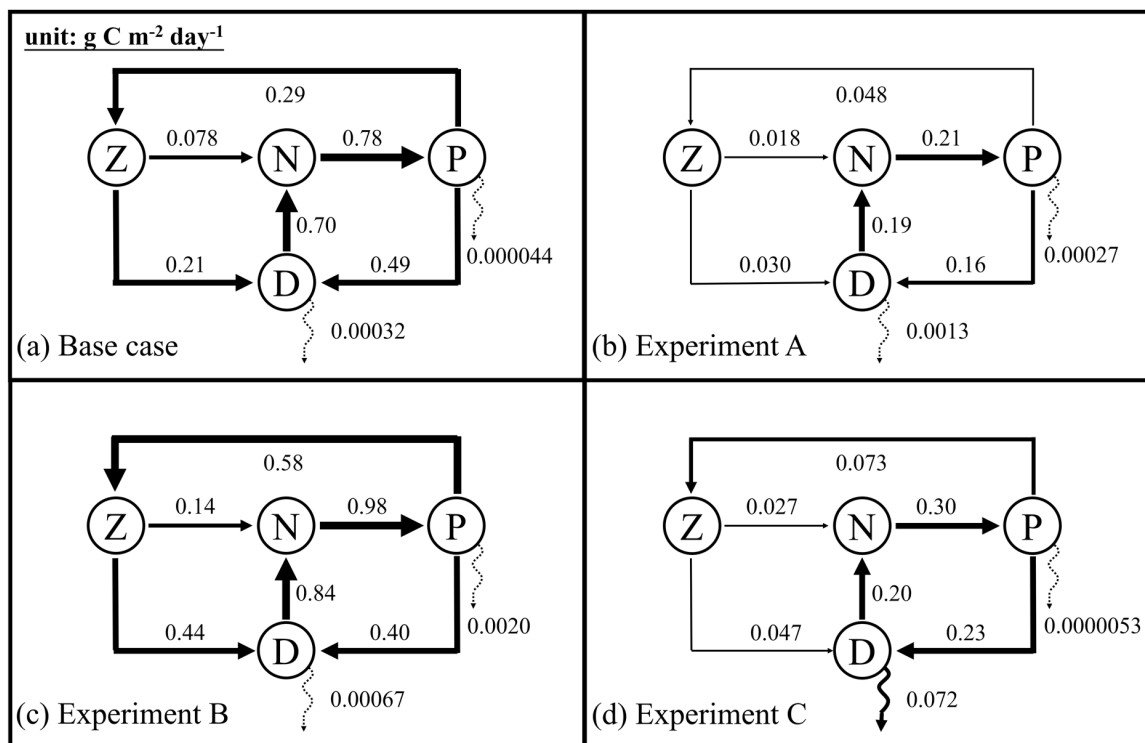
Figure 6. Annually averaged carbon fluxes integrated over the upper 200 m (unit: g C m^{-2} day^{-1}) for the base case (a) and optimized experiments A, B, and C. The N, P, Z, and D stand for the pools of nutrient, phytoplankton, zooplankton, and the sum of small and large detritus, respectively. The thickness of arrows scales with the magnitude of fluxes. Dashed arrows represent fluxes lower than 0.01 g C m^{-2} day^{-1}.
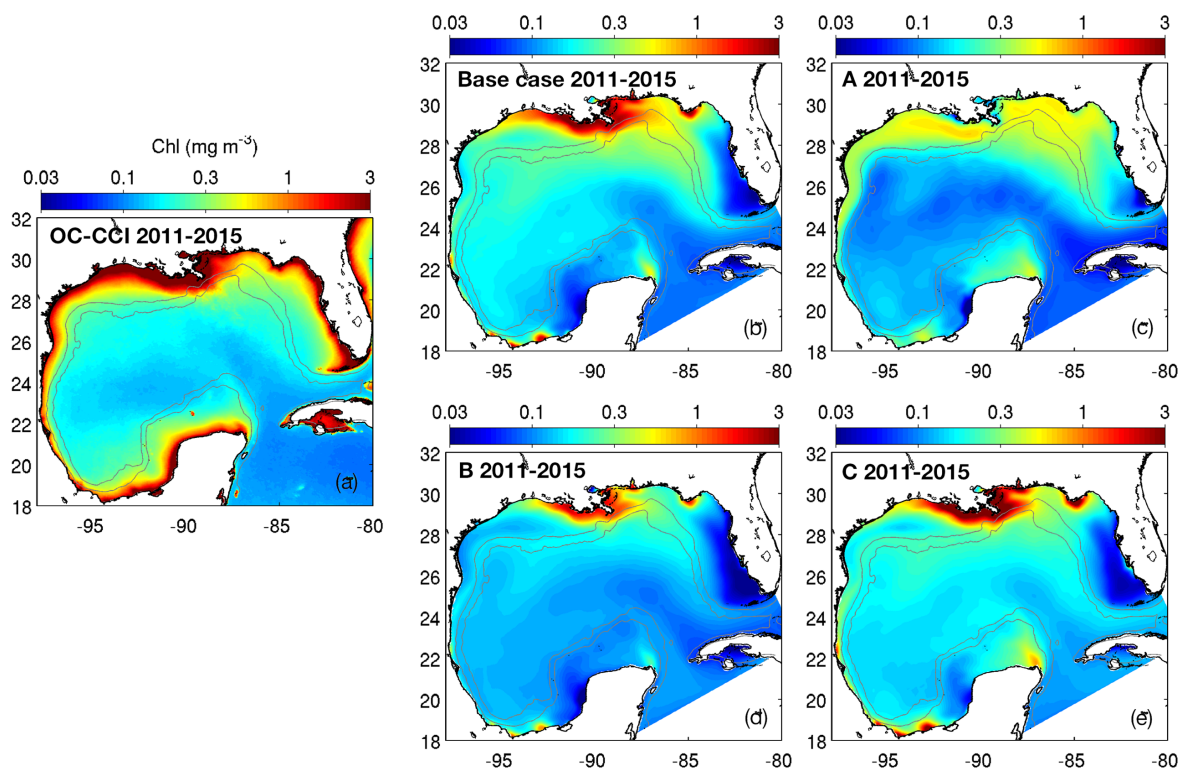
Figure 7. Spatial distributions of the annual mean chlorophyll in the surface layer from the satellite (OC-CCI) climatology (2011-2015) and the different model versions. The gray contours mark the bathymetric depths of 200 and 1000 m.
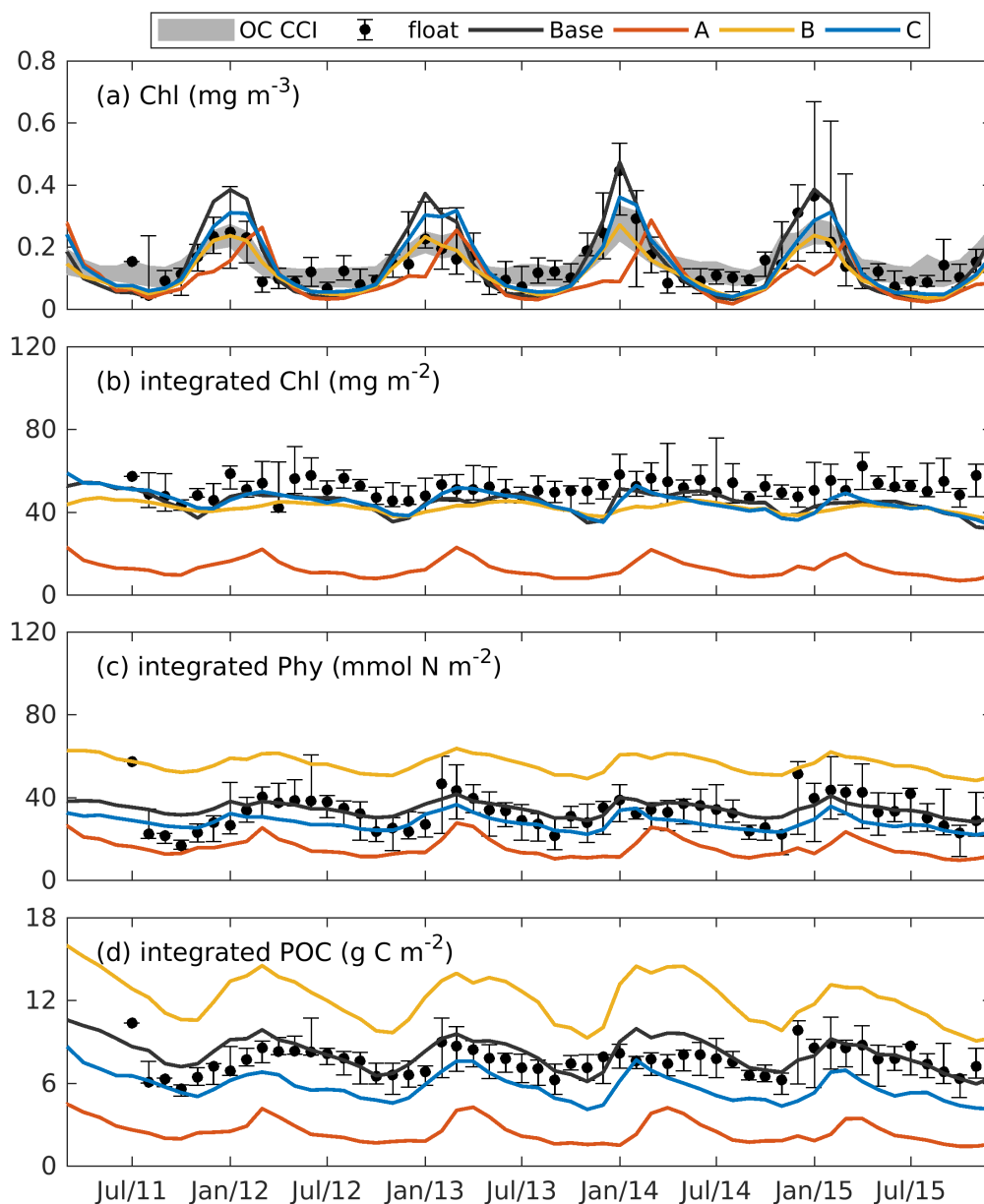
Figure 8. Observed and simulated seasonal cycles of surface chlorophyll (a), vertically integrated chlorophyll (b), vertically integrated phytoplankton (c), and vertically integrated POC (d) from each 3D models. Solid lines represent the median values over the deep ocean of GOM (depth>1000m). Error bars and shades show the 25% and 75% percentiles. Chlorophyll, phytoplankton, and POC are integrated over the top 200m.
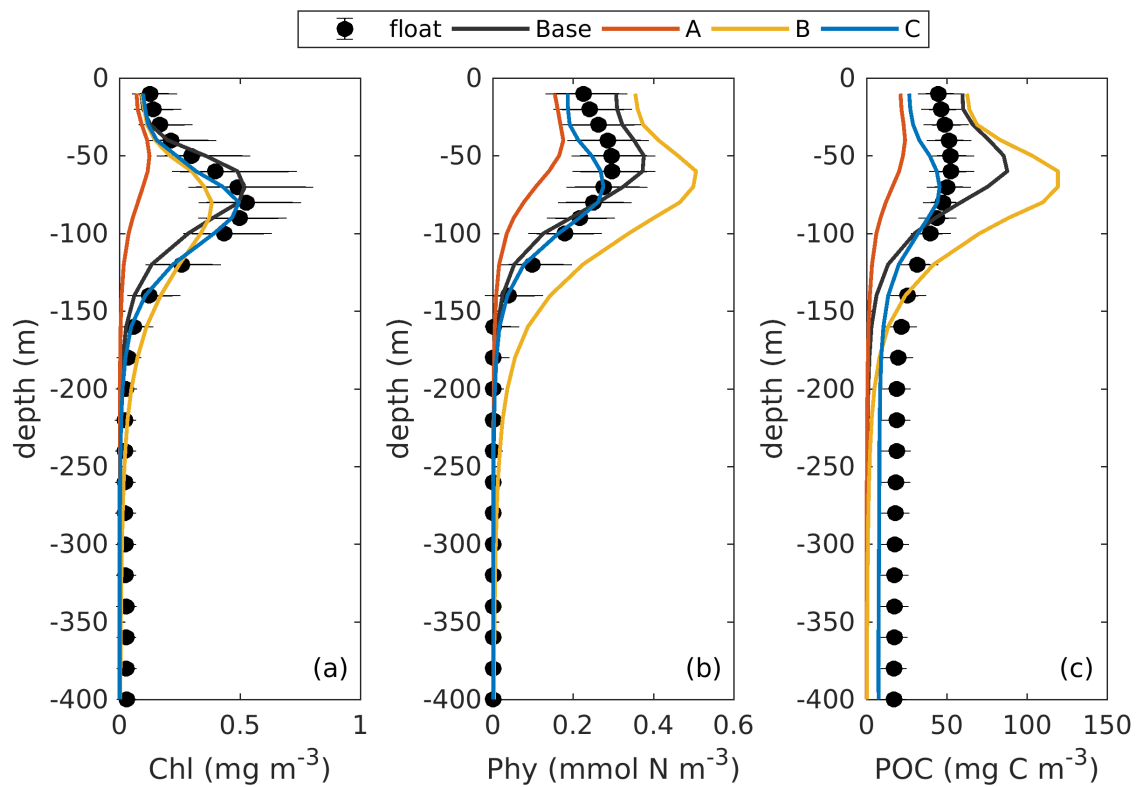
Figure 9. Observed and simulated vertical profiles of chlorophyll, phytoplankton, and POC from each 3D models.
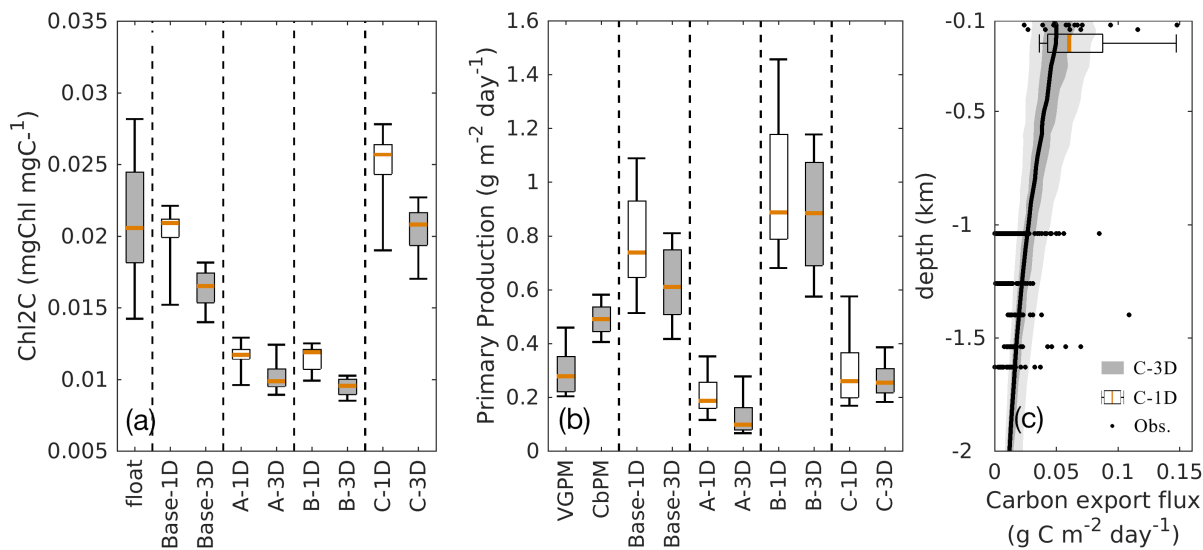
Figure 10. Comparisons of the chlorophyll to carbon ratio (a), primary production (b), and carbon export fluxes (c) between the 1D and 3D models.